NEUROSCIENCE

Integrated proteomics reveals brain-based cerebrospinal fluid biomarkers in asymptomatic and symptomatic Alzheimer's disease

Lenora Higginbotham[1,2,3]*, Lingyan Ping[2,3,4]*, Eric B. Dammer[2,3,4], Duc M. Duong[2,3,4], Maotian Zhou[2,3,4], Marla Gearing[1,3,5], Cheyenne Hurst[2], Jonathan D. Glass[1,2,3], Stewart A. Factor[1], Erik C. B. Johnson[1,2,3], Ihab Hajjar[1,3], James J. Lah[1,2,3], Allan I. Levey[1,2,3†], Nicholas T. Seyfried[1,2,3,4†]

Alzheimer's disease (AD) lacks protein biomarkers reflective of its diverse underlying pathophysiology, hindering diagnostic and therapeutic advancements. Here, we used integrative proteomics to identify cerebrospinal fluid (CSF) biomarkers representing a wide spectrum of AD pathophysiology. Multiplex mass spectrometry identified ~3500 and ~12,000 proteins in AD CSF and brain, respectively. Network analysis of the brain proteome resolved 44 biologically diverse modules, 15 of which overlapped with the CSF proteome. CSF AD markers in these overlapping modules were collapsed into five protein panels representing distinct pathophysiological processes. Synaptic and metabolic panels were decreased in AD brain but increased in CSF, while glial-enriched myelination and immunity panels were increased in brain and CSF. The consistency and disease specificity of panel changes were confirmed in >500 additional CSF samples. These panels also identified biological subpopulations within asymptomatic AD. Overall, these results are a promising step toward a network-based biomarker tool for AD clinical applications.

INTRODUCTION

Alzheimer's disease (AD), the most common cause of neurodegenerative dementia worldwide, is characterized by dysfunction in a wide range of biological systems, including synaptic transmission, glial-mediated immunity, and mitochondrial metabolism (*1*–*3*). However, its established protein biomarkers remain focused on the detection of amyloid and tau pathology and hence fail to reflect this diverse pathophysiology. These "core" protein biomarkers, most reliably measured in the cerebrospinal fluid (CSF), include (i) amyloid-beta peptide 1-42 ($A\beta_{1-42}$), reflective of cortical amyloid plaque formation; (ii) total tau, a marker of axonal degeneration; and (iii) phospho-tau (p-tau), representative of pathological tau hyperphosphorylation (*4*–*7*). While these CSF biomarkers have greatly advanced our detection of "hallmark" AD proteinopathy (*4*–*7*), they represent only a fraction of the intricate biology underlying the disease.

This lack of pathophysiological diversity among AD biomarkers contributes to numerous challenges, including (i) an inability to recognize and quantify biological heterogeneity among patients with AD, (ii) inadequate measures of disease severity and progression, especially in preclinical stages, and (iii) therapeutic drug development that fails to fully address all aspects of neurological deterioration. Our reliance on hallmark pathology to delineate AD from related conditions only exacerbates these issues. Increasing evidence suggests that most demented elderly individuals harbor more than one hallmark pathology of cognitive decline (*8*). Up to 90% or more of individuals with AD pathology feature concurrent vascular disease, TDP-43 inclusions, or other degenerative pathologies (*9*). These high rates of overlapping pathologies undermine our current diagnostic framework of dementia and necessitate more pathophysiologically comprehensive definitions of disease.

Given this urgent need for diverse AD biomarkers, the field has increasingly embraced holistic systems-based "omics" approaches to biomarker discovery. Launched in 2014, the Accelerating Medicines Partnership (AMP)–AD consortium is at the forefront of this initiative. This multidisciplinary effort among the National Institutes of Health, academia, and industry aims to leverage systems-based strategies to better define AD pathophysiology and develop biologically diverse diagnostic assays and therapeutic strategies (*10*). As part of this initiative, network proteomics has emerged as a promising tool for systems-based biomarker advancement in AD. This unbiased data-driven approach organizes complex proteomic datasets into groups or "modules" of coexpressed proteins with links to specific cell types, organelles, and biological functions (*11*–*13*). Nearly a dozen informative network proteomic studies have now been performed on the AD brain (*13*–*23*). Collectively, these analyses demonstrate that the AD brain network proteome maintains a highly conserved module organization across independent cohorts and multiple cortical regions. In addition, several of these modules demonstrate reproducible AD-associated abundance changes across datasets, reflecting a diverse range of disease pathophysiologies. Overall, these findings showcase the brain network proteome as a promising anchor for systems-based biomarker discovery in AD.

To advance the translation of the AD brain network proteome into clinically useful systems-based biomarkers, we integrated this brain-derived network with proteomic analysis of AD CSF. This integrative approach resulted in the identification of five panels of promising CSF biomarkers linked to a wide range of brain-based

[1]Department of Neurology, Emory University School of Medicine, Atlanta, GA, USA. [2]Center for Neurodegenerative Disease, Emory University School of Medicine, Atlanta, GA, USA. [3]Goizueta Alzheimer's Disease Research Center, Emory University, Atlanta, GA, USA. [4]Department of Biochemistry, Emory University School of Medicine, Atlanta, GA, USA. [5]Department of Pathology and Laboratory Medicine, Emory University School of Medicine, Atlanta, GA, USA.
*These authors contributed equally to this work.
†Corresponding author. Email: nseyfri@emory.edu (N.T.S.); alevey@emory.edu (A.I.L.)

pathophysiology, including dysfunction in synaptic, vascular, myelination, inflammatory, and metabolic pathways. We successfully validated these biomarker panels across multiple replication analyses, comprising more than 500 CSF samples from a variety of neurodegenerative conditions. These validation analyses included the examination of panel targets in the CSF of individuals with asymptomatic AD (AsymAD), or those displaying evidence of aberrant amyloid accumulation in the setting of normal cognition. These analyses highlighted notable biological heterogeneity within the AsymAD population and identified panel markers potentially capable of subtyping individuals in the earliest stages of illness. Overall, these results represent a critical step toward the development of a diverse systems-based protein biomarker tool that could successfully address many of the clinical challenges facing AD.

RESULTS

CSF proteome reveals markers significantly altered in AD

The main objective of this study was to identify novel CSF biomarkers reflective of the diverse brain-based pathophysiologies that contribute to AD. Figure S1 provides an overview of our study approach, which comprised (i) an initial discovery-driven integrative analysis of AD CSF and network brain proteomes to identify a diverse group of brain-linked CSF biomarkers of disease and (ii) the subsequent replication of these biomarkers in several independent CSF cohorts. The discovery-driven investigations began with differential expression analysis of CSF from 20 cognitively normal individuals and 20 individuals with AD of the Emory Goizueta Alzheimer's Disease Research Center (ADRC). AD diagnoses were defined by significant cognitive impairment [mean Montreal Cognitive Assessment (MoCA), 13.8 ± 7.0] in the setting of low $A\beta_{1-42}$ and elevated total tau and p-tau levels in the CSF [enzyme-linked immunosorbent assay (ELISA)] (table S1A). Controls (mean MoCA, 26.7 ± 2.2) featured normal levels of CSF biomarkers.

Human CSF is characterized by a dynamic range of protein abundance, in which albumin and other exceedingly highly abundant proteins can prevent the detection of proteins of interest (*24*). To increase the depth of protein discovery, we depleted the top 14 highly abundant proteins from each CSF sample before mass spectrometry (MS) analysis (*24*). In total, MS identified 39,805 peptides mapping to 3691 protein groups across the 40 samples. Quantification of proteins was performed via multiplex tandem mass tag (TMT) labeling (*18*, *25*). To account for missing data, we included only those proteins quantified in at least 50% of samples in subsequent analyses, resulting in the final quantification of 2875 protein groups. Because of notable differences in total protein abundance levels, one control sample was statistically deemed an outlier (*13*) and not included in subsequent analyses. The abundance values of the remaining 39 samples were adjusted for age, sex, and batch covariance (*13*–*15*, *17*, *18*, *20*, *26*).

Differential expression was assessed on the post-regressed dataset using a statistical *t* test analysis, which identified proteins with significantly altered abundance levels ($P < 0.05$) between control and AD cases (table S2A). As demonstrated in Fig. 1A, there were a total of 225 proteins with significantly decreased abundance and 303 proteins with significantly increased abundance in AD. These differentially expressed proteins included several previously identified CSF AD markers, such as microtubule-associated protein tau (MAPT; $P = 3.52 \times 10^{-8}$), neurofilament light (NEFL; $P = 6.56 \times 10^{-3}$), growth-associated protein 43 (GAP43; $P = 1.46 \times 10^{-5}$), fatty acid–binding protein 3 (FABP3; $P = 2.00 \times 10^{-5}$), chitinase 3 like 1 (CHI3L1; $P = 4.44 \times 10^{-6}$), neurogranin (NRGN; $P = 3.43 \times 10^{-4}$), and VGF nerve growth factor (VGF; $P = 4.83 \times 10^{-3}$) (*4*–*6*). However, we also identified other highly significant targets, such as GDP dissociation inhibitor 1 (GDI1; $P = 1.54 \times 10^{-10}$) and SPARC-related modular calcium binding 1 (SMOC1; $P = 6.93 \times 10^{-9}$). Gene ontology (GO) analysis of the 225 significantly decreased proteins revealed strong links to humoral processes, such as steroid metabolism, coagulation, and hormone activity (Fig. 1B and table S2B). Conversely, the 303 significantly increased proteins were strongly associated with cell structure and energy metabolism.

Proteomic levels of MAPT correlated strongly to independently measured ELISA tau levels ($r = 0.78$, $P = 7.8 \times 10^{-9}$; Fig. 1C), supporting the validity of our MS measurements. Isoform-specific peptides mapping to the C terminus of $A\beta_{1-40}$ and $A\beta_{1-42}$ do not ionize efficiently following tryptic digestion of amyloid precursor protein (APP) levels (*27*, *28*). Therefore, the APP peptides we identified were not correlated to ELISA $A\beta_{1-42}$ levels. To assess differential expression across individual cases, we used differentially expressed proteins with $P < 0.0001$ [false discovery rate (FDR)–corrected $P < 0.01$] to perform a supervised cluster analysis across samples (table S2A). As shown in Fig. 1D, these 65 highly significant proteins were able to correctly cluster samples by disease status except for one AD case with a control-like profile. Of these 65 proteins, 63 were increased in AD, while only two (CD74 and ISLR) were decreased. Overall, these CSF analyses identified hundreds of altered proteins in AD that could potentially serve as biomarkers of disease.

Network brain proteome reveals modules linked to AD neuropathology

We then performed an independent network analysis of the AD brain proteome. This discovery brain cohort comprised dorsolateral prefrontal cortex (DLPFC) samples from control ($n = 10$), Parkinson's disease (PD; $n = 10$), mixed AD/PD ($n = 10$), and AD ($n = 10$) cases of the Emory Goizueta ADRC. The demographics of these 40 cases have been previously described (*25*) and are summarized in table S1B. We analyzed these 40 brain tissues, as well as a replication cohort of 27 cases, using TMT-MS. Collectively, both brain datasets yielded 227,121 unique peptides mapping to 12,943 protein groups (*25*). Only those proteins quantified in at least 50% of cases were included in subsequent investigations. The final discovery dataset comprised 8817 quantified proteins. Protein abundance levels were adjusted for age, sex, and postmortem interval (PMI). Differential expression analysis of the post-regressed dataset revealed >2000 proteins with significantly altered levels [$P < 0.05$, analysis of variance (ANOVA)] across two or more disease cohorts. We then performed a supervised cluster analysis based on differentially expressed proteins with $P < 0.0001$ across AD/control and/or AD/PD comparisons (fig. S2, A and B, table S2C). These 165 highly altered proteins sharply delineated cases harboring AD pathology from control and PD samples, confirming robust AD-specific changes across the proteome.

We subsequently performed a network analysis of the discovery brain proteome using an algorithm called weighted gene coexpression network analysis (WGCNA), which organizes the dataset into modules of proteins with similar expression patterns across cases (*11*–*13*). This analysis identified 44 modules (M) of coexpressed proteins ranked and numbered according to size from largest (M1, $n = 1821$ proteins) to smallest (M44, $n = 34$ proteins) (Fig. 2A and

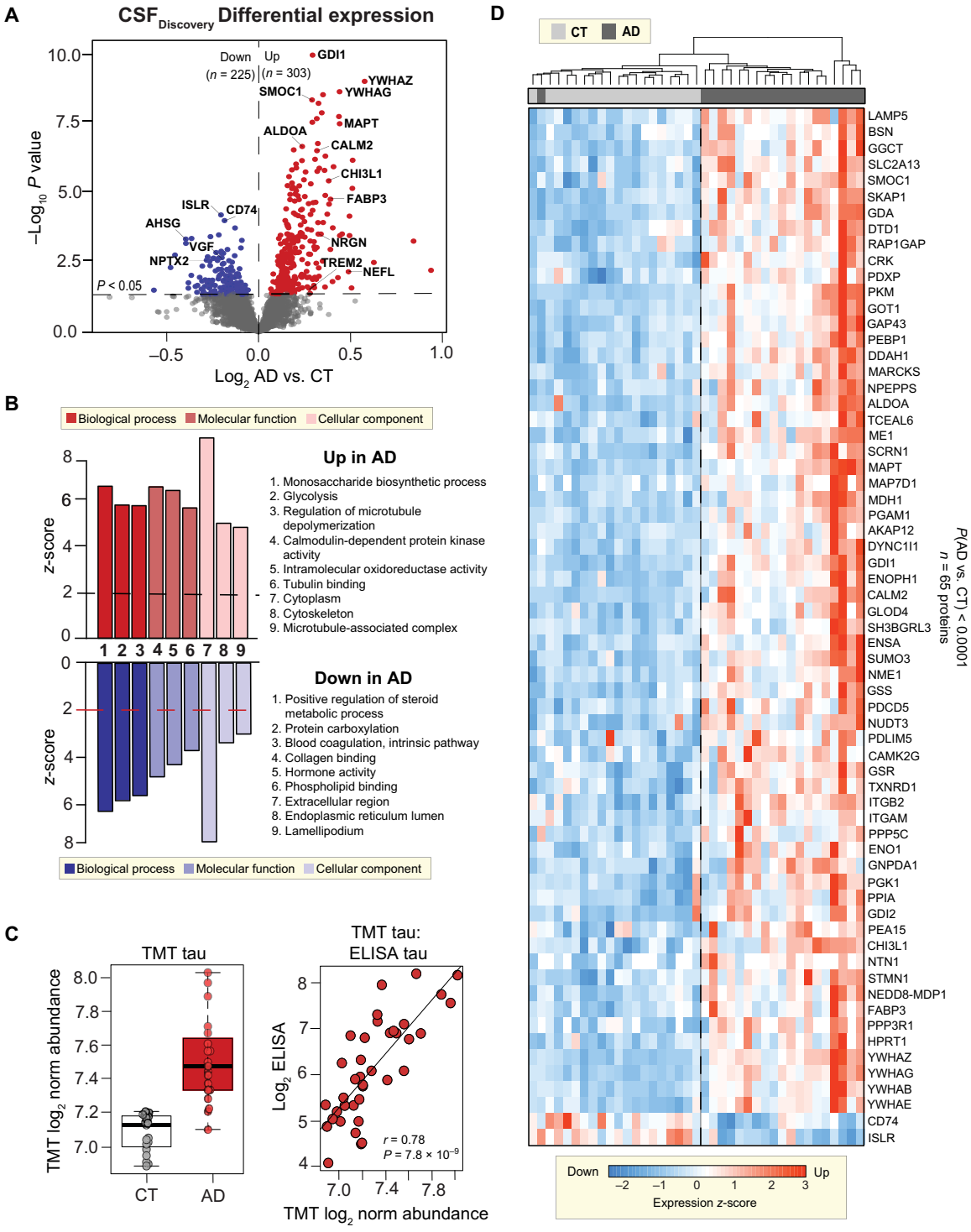

Fig. 1. Differential expression of discovery CSF proteome. (**A**) Volcano plot displaying the $\log_2$ fold change (*x* axis) against the *t* test–derived $-\log_{10}$ statistical *P* value (*y* axis) for all proteins differentially expressed between control (CT) and AD cases of the CSF discovery proteome. Proteins with significantly decreased levels in AD ($P < 0.05$) are shown in blue, while the proteins with significantly increased levels in disease are noted in red. Select proteins are labeled. (**B**) Top GO terms associated with proteins significantly decreased (blue) and increased (red) in AD. The three GO terms with the highest *z*-scores in the domains of biological process, molecular function, and cellular component are shown. (**C**) MAPT levels in the discovery CSF samples measured by MS (left) and their correlations to sample ELISA tau levels (right). Pearson correlation coefficient with associated *P* value is shown. Because of missing ELISA data for one AD case, these plots included values across 38 of the 39 analyzed cases. (**D**) Supervised cluster analysis across the control and AD CSF discovery samples using the 65 most significantly altered proteins in the dataset ($P < 0.0001$, Benjamini-Hochberg (BH)–corrected $P < 0.01$). Norm, normalized.

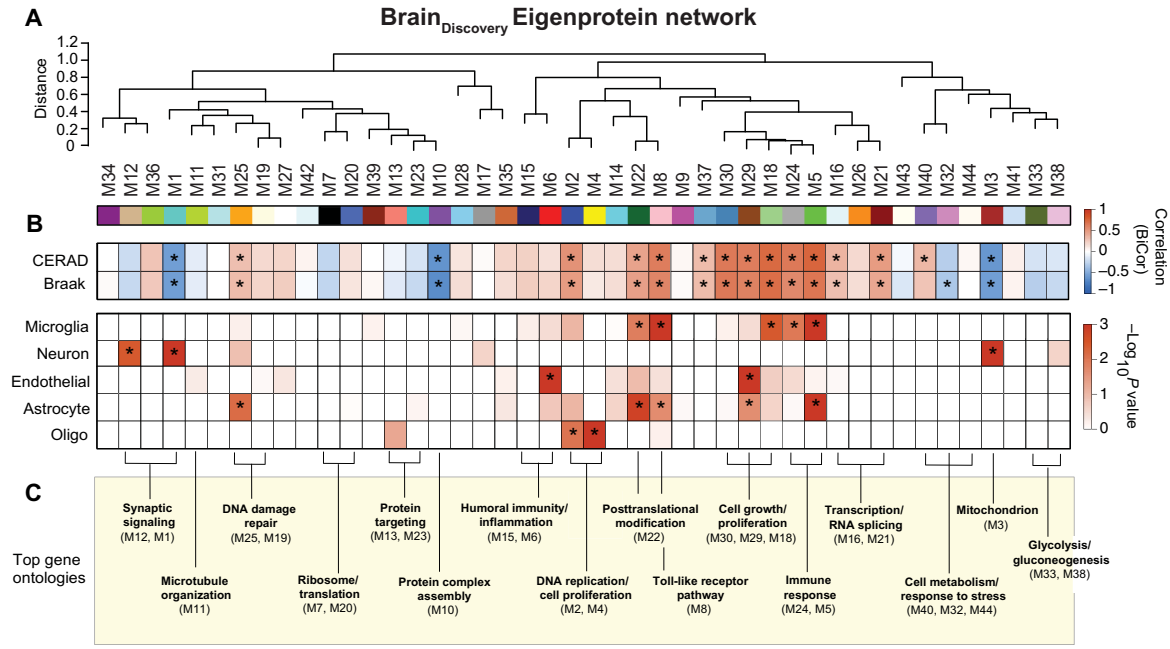

Fig. 2. Network analysis of the discovery brain proteome. (**A**) WGCNA of the discovery brain proteome. (**B**) Biweight midcorrelation (BiCor) analysis of module eigenproteins (the first principle components of module protein expression) with neuropathological hallmarks of AD (top), including CERAD (Aβ plaque) and Braak (tau tangle) scores. The strengths of positive (red) and negative (blue) correlations are shown by two-color heatmap with asterisks denoting statistical significance ($P < 0.05$). The cell type associations of each protein module were assessed using a hypergeometric Fisher's exact test (FET) (bottom). The strength of the red shading indicates the degree of cell type enrichment with asterisks denoting statistical significance ($P < 0.05$). The FET-derived P values were corrected using the BH method. (**C**) GO analysis of module proteins. The most strongly associated biological processes are shown for each module or group of related modules. oligo, oligodendrocyte.

table S2D). Representative expression profiles, or eigenproteins, were calculated for each module as previously described (*13*) and correlated to disease status and AD pathology, i.e., Consortium to Establish a Registry for Alzheimer's Disease (CERAD) and Braak scores (Fig. 2B). Overall, there were 17 modules that correlated significantly to AD neuropathology ($P < 0.05$). Many of these disease-associated modules were also strongly enriched with cell type–specific markers (Fig. 2B). As previously described (*13*), cell type enrichment was determined by analyzing module overlap with reference lists of cell type–specific genes derived from published RNA sequencing (RNA-seq) experiments in isolated murine neuronal, endothelial, and glial cells (*29*).

A cluster of five closely related astrocyte- and microglia-enriched modules (M30, M29, M18, M24, and M5) demonstrated strong positive correlations to AD neuropathology (Fig. 2B). Ontological analysis linked these glial modules to cell growth, proliferation, and immunity (Fig. 2C and table S2E). Two additional glial modules, M8 and M22, were also strongly up-regulated in disease. M8 was highly associated with the Toll-like receptor pathway, a signaling cascade that plays a critical role in the innate immune response (*30*). Meanwhile, M22 was strongly linked to posttranslational modification. The oligodendrocyte-enriched M2 demonstrated strong positive correlations to AD pathology and ontological links to nucleoside synthesis and DNA replication, suggesting heightened cell proliferation in disease. Overall, these findings supported the glial module elevations we have previously observed in the AD network proteome (*13*, *17*). Many of the AD-associated glial modules in the current discovery network showed lower expression levels in control and PD cases, highlighting the disease specificity underlying their elevations in AD (fig. S2C).

There were only four modules (M1, M3, M10, and M32) in our network proteome with strong negative correlations to AD pathology ($P < 0.05$) (Fig. 2, B and C). M1 and M3 were both enriched with neuronal markers. While M1 was highly associated with synaptic signaling, M3 was strongly linked to mitochondrial function. M10 and M32 featured no evidence of cell type enrichment. M32 mirrored M3 in its links to cellular metabolism, while M10 was highly associated with cell growth and microtubule function. All four of these modules were increased in controls and PD compared to AD, conferring disease specificity to their AD changes (fig. S2C). Overall, these results supported the decreased abundance of neuronal-enriched modules we have previously observed in AD (*13*, *17*). In summary, network analysis of our discovery brain proteome yielded modules with AD-specific alterations consistent with our prior findings.

Disease-related brain modules are preserved in AsymAD

AD is characterized by an early, asymptomatic phase (AsymAD) in which individuals exhibit amyloid accumulation in the absence of clinical cognitive decline (*5*, *31*). This asymptomatic stage represents a critical window for early detection and intervention. We have previously demonstrated strong module preservation of AsymAD and AD brain network proteomes across independent datasets (*13*, *17*). To ensure our current discovery brain network aligned with these previous findings, we analyzed the preservation of our 44 modules in a replication dataset derived from 27 DLPFC tissues comprising control ($n = 10$), AsymAD ($n = 8$), and AD ($n = 9$) cases. The control and AD samples were among those included in the analysis in our discovery brain cohort (table S1B), while the AsymAD cases were unique to only the replication cohort. These AsymAD cases, also derived from the Emory Goizueta ADRC brain bank, featured abnormally high amyloid levels (mean CERAD, 2.8 ± 0.5) despite normal cognition at death (table S1B).

TMT-MS analysis of these 27 brain tissues resulted in the quantification of 11,244 protein groups. This final count included only those proteins quantified in at least 50% of samples. This replication dataset comprised 8638 of the 8817 proteins (98.0%) detected in our discovery brain analysis and featured nearly 3000 significantly altered proteins ($P < 0.05$, post-ANOVA Tukey pairwise *t* test) between the control and AD cohorts (table S2F). Of these differentially expressed proteins, 910 also demonstrated significantly altered levels between AD and control cases of the discovery brain proteome ($P < 0.05$, post-ANOVA Tukey pairwise *t* test). Notably, these 910 markers were highly consistent in their direction of change between proteomes ($r = 0.94$, $P < 1.0 \times 10^{-200}$) (fig. S3A). Among increased proteins, those featuring the most concordant changes between datasets were largely members of the glial-enriched M5 and M18 modules (MDK, COL25A1, MAPT, NTN1, SMOC1, and GFAP). Among decreased proteins, those with the most concordant changes were almost exclusively members of the synapse-associated M1 module (NPTX2, VGF, and RPH3A). We further validated the AD-associated alterations of midkine (MDK), CD44, secreted frizzled related protein 1 (SFRP1), and VGF by immunoblotting (fig. S3B). Module preservation analysis demonstrated that approximately 80% of protein modules (34/44) in the discovery brain proteome were significantly conserved (*z*-score > 1.96, FDR-corrected $P < 0.05$) in the replication dataset (fig. S3C). Fourteen of these modules were exceptionally preserved (*z*-score > 10, FDR-corrected $P < 1.0 \times 10^{-23}$) between the two proteomes. Overall, the high agreement in differential expression and module composition between the discovery and replication brain proteomes highlighted the reproducibility of protein alterations in the AD frontal cortex. In addition, it confirmed that AsymAD and more advanced disease share a very similar brain network structure.

A more detailed analysis of differential expression in the brain replication dataset highlighted a notable degree of AsymAD protein alterations, including a total of 151 significantly altered proteins ($P < 0.05$) between AsymAD and controls (fig. S3D). Concordant with amyloid burden, APP was significantly elevated in both the AsymAD and AD brain. MAPT was significantly altered only in AD, consistent with increased tangle levels and their known correlation to cognitive decline (*5*, *7*). Glial-enriched modules (M5 and M18) were highly reflected among proteins increased in AsymAD, while the neuronal-linked M1 module was most represented among proteins decreased in AsymAD. Many of these AsymAD markers demonstrated even greater changes in symptomatic disease. Among these markers was SMOC1, a glial protein belonging to M18 with links to brain tumors and eye and limb development (*32*). MDK, a heparin-binding growth factor linked to cell growth and angiogenesis (*33*), was another M18 member that demonstrated significant increases in AsymAD compared to controls, followed by even greater increases in AD. In contrast, the synaptic protein neuropentraxin 2 (NPTX2) was significantly decreased in the AsymAD brain. NPTX2 has been previously linked to neurodegeneration and has a well-established role in mediating the excitatory synapse (*34*). Overall, these results revealed a diverse range of preclinical protein changes in AD that appear to progress with disease severity.

Overlap between brain protein and RNA networks reveals shared and protein-specific module changes in AD

Given the significant depth of protein coverage we achieved in our discovery brain proteome, we sought to gain a more comprehensive understanding of its overlap with the AD transcriptome at the network level. We thus compared the module overlap between our discovery brain proteome and an RNA network we previously generated from the microarray measurements of 18,204 genes across AD ($n = 308$) and control ($n = 157$) DLPFC tissues (*13*). We identified a total of 20 distinct RNA modules, many demonstrating enrichment for specific cell types, including neurons, oligodendrocytes, astrocytes, and microglia (Fig. 3A). The fold change of these modules in AD is shown in Fig. 3B. Consistent with a prior protein-RNA overlap analysis we performed using a less deep label-free MS proteome (~3000 proteins) (*13*), the majority of the 44 modules in our discovery brain proteome network did not significantly overlap in transcriptome network. Even among those 34 protein modules highly preserved across our discovery and replication brain proteomes, only 14 (~40%) demonstrated statistically significant overlap with the transcriptome by Fisher's exact test (FET) (Fig. 3A). Several protein modules associated with DNA damage repair (P-M25 and P-M19), protein translation (P-M7 and P-M20), RNA binding/splicing (P-M16 and P-M21), and protein targeting (P-M13 and P-M23) did not overlap with modules in the transcriptome. Therefore, despite using a much deeper proteomic dataset in the current overlap analysis (*13*), the bulk of the AD network proteome did not map to the transcriptomic network.

Most of the overlapping protein and RNA modules shared similar cell type enrichment profiles and consistent directions of change in AD (Fig. 3, B and C). Namely, the synapse-associated M1 module of the brain proteome (P-M1) mapped to three neuron-enriched cognate RNA modules (R-M1, R-M9, and R-M16), which all demonstrated decreased levels in AD. Likewise, the glial-enriched M5 and M18 protein modules overlapped with RNA modules enriched with astrocytic and microglial markers (R-M3, R-M7, and R-M10) and highly increased in disease. These shared module characteristics between the two datasets further support the cell type enrichment and disease-associated changes we observed in our brain proteomes. However, we observed many notable differences between the RNA and protein levels of individual markers within these shared modules. A correlation analysis of the proteomic and transcriptomic differential expression of molecules within these overlapping modules (Fig. 3D) highlighted this discordance. For example, APP and several other glial module proteins (NTN1, MDK, COL25A1, ICAM1, and SFRP1) demonstrated substantial increases in the AD proteome, but little to no change in the AD transcriptome. These protein-specific changes, likely a result of strong associations with amyloid plaques (*23*, *35*), highlight the proteome as a source of pathological alterations that may not be reflected in the transcriptome.

Integration of AD brain and CSF proteomes yields fluid biomarker panels reflective of brain network pathology

After independently analyzing our discovery brain and CSF proteomes, we then applied an integrative analysis to the two datasets to identify AD CSF biomarkers linked to brain network pathophysiology. It was first essential that we define the overlap of the two proteomes. While it is well accepted that the CSF mirrors neurochemical changes in the AD brain (*4*), the precise degree of overlap between the AD brain and CSF proteomes is unclear. By comparing the number of shared gene products detected among our two proteomes, we found that nearly 70% ($n = 1936$) of proteins identified in the CSF were also quantified in the brain (Fig. 4A). The bulk of these overlapping proteins ($n = 1721$) mapped to one of the 44 coexpression modules derived from the discovery brain dataset (Fig. 4B). As

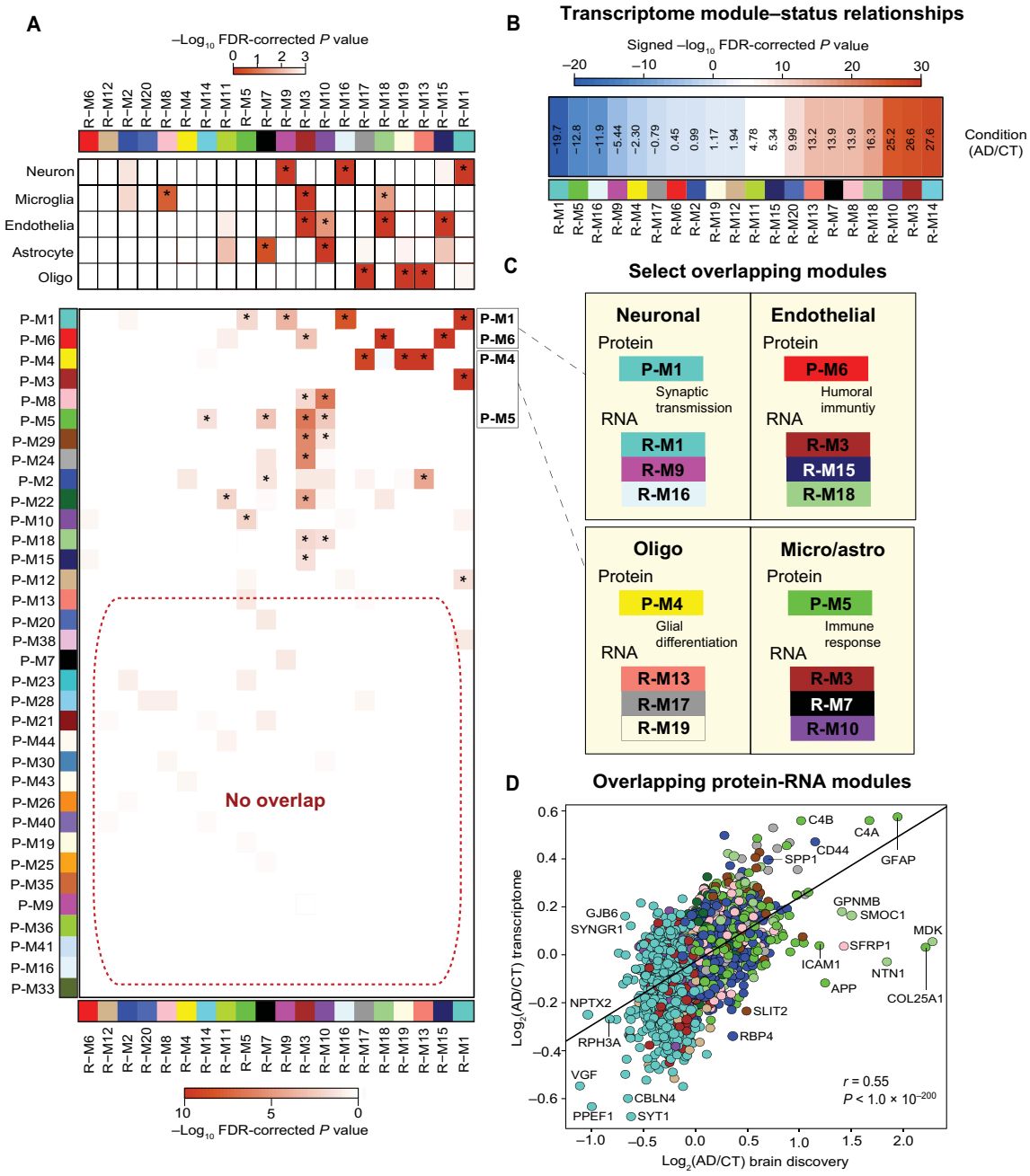

Fig. 3. Overlap between protein and RNA coexpression networks in AD. (**A**) Hypergeometric FETs demonstrating enrichment of cell type–specific markers within RNA modules of the AD transcriptome (top) and degree of overlap between RNA (*x* axis) and protein (*y* axis) modules of the AD brain (bottom). The strength of red shading indicates the degree of cell type enrichment in the top panel and strength of module overlap in the bottom panel. Asterisks denote statistical significance ($P < 0.05$). (**B**) Degree of correlation between each transcriptome module eigengene and AD status with those modules most negatively correlated to AD on the left (blue) and those most positively correlated to AD on the right (red). Log-transformed BH-corrected *P* value indicates degree of statistical significance for each correlation. (**C**) Notable overlapping modules with shared cell type enrichment. (**D**) Correlation analysis of the protein (*x* axis) and RNA (*y* axis) $\log_2$ fold changes of markers within overlapping modules. Pearson correlation coefficient with associated *P* value is shown. Micro, microglia; astro, astrocyte. CT, control.

expected, the six largest brain modules (M1 to M6) demonstrated the greatest amount of CSF overlap. However, there were smaller brain modules (e.g., M15 and M29) that achieved an unexpectedly high degree of overlap, greater than brain modules twice their size. This prompted us to take a more detailed, statistically driven approach to calculating overlap between the brain and CSF.

Using a one-tailed FET, we assessed the significance of protein overlap between the CSF proteome and individual brain modules. This analysis revealed a total of 14 brain modules with statistically significant overlap in the discovery CSF dataset (FDR-corrected $P < 0.05$), as well as one additional module (M18) whose extent of overlap approached significance (FDR-corrected $P = 0.06$) (Fig. 4C, top row).

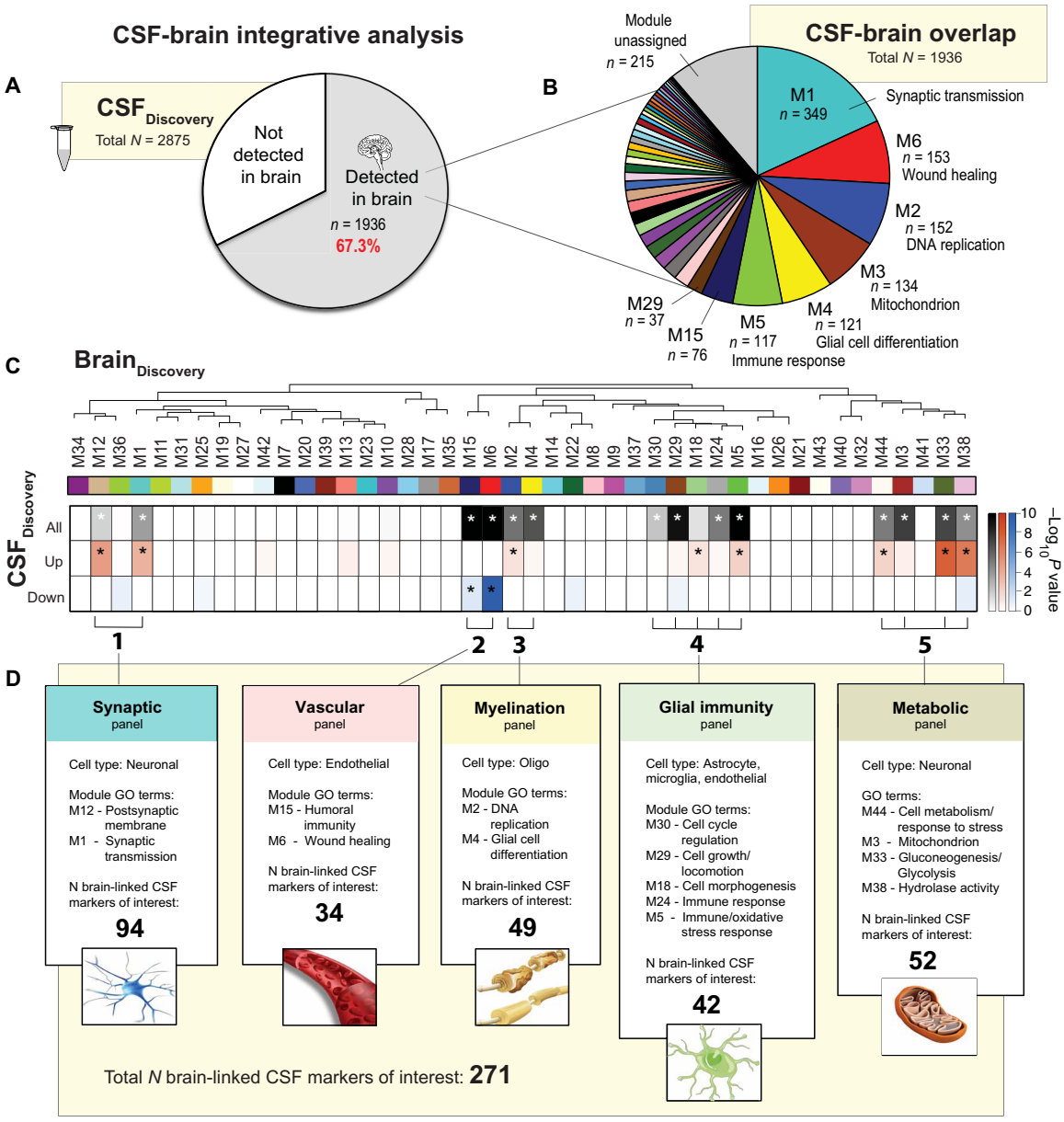

Fig. 4. Integrative analysis of CSF and brain proteomes yields panels of brain-linked CSF AD biomarkers. (**A** and **B**) Overlap of proteins detected in the discovery brain and CSF datasets. Most of these overlapping proteins were linked to 1 of the 44 coexpression modules of the brain coexpression network. (**C**) Overlap between the discovery CSF proteome and discovery brain network proteome. Each line of the heatmap represents a separate overlap analysis by hypergeometric FET. The top row depicts the overlap (gray/black shading) between brain modules and the entire CSF proteome. The second row depicts the overlap (red shading) between brain modules and CSF proteins significantly up-regulated in AD ($P < 0.05$). The third row demonstrates the overlap (blue shading) between brain modules and CSF proteins significantly down-regulated in AD ($P < 0.05$). The FET-derived P values were corrected using the BH method. (**D**) Collapsed module panels based on cell type associations and related GO terms. These panels comprised a total of 271 brain-linked proteins with meaningful differential expression in the CSF proteome.

We were also interested in modules that overlapped strongly with differentially expressed CSF proteins. Therefore, we applied two additional FET analyses to determine those brain modules with meaningful overlap among (i) CSF proteins significantly increased in AD and (ii) CSF proteins significantly decreased in AD ($P < 0.05$, pairwise t test AD/control). As shown in the middle and bottom rows of Fig. 4C, these additional analyses revealed that 8 of the 44 brain modules significantly overlapped with proteins increased in AD CSF (M12, M1, M2, M18, M5, M44, M33, and M38), while only two modules (M6 and M15) demonstrated meaningful overlap with proteins decreased in AD CSF. As expected, all 10 of these modules were among the 15 modules with the highest degree of overlap with the CSF proteome. We therefore hypothesized that these 15 modules were collectively high-yield sources of brain-derived CSF biomarkers of AD.

We collapsed these 15 overlapping modules into five large protein panels based on their adjacency in the WGCNA dendrogram and associations with cell types and gene ontologies (Fig. 4D). The first

panel comprised modules strongly enriched with neuronal markers and synapse-associated proteins (M1 and M12). This synaptic panel contained a total of 94 proteins with significantly altered levels in the CSF proteome, making it the largest source of brain-linked CSF markers among the five panels. The second panel (M6 and M15) demonstrated strong links to endothelial cell markers and vascular ontologies, such as "wound healing" (M6) and "regulation of humoral immune response" (M15). M15 was also highly linked to lipoprotein metabolism, a process intimately associated with the endothelium (*36*). This vascular panel harbored 34 brain-linked CSF markers. The third panel comprised modules (M2 and M4) significantly linked to oligodendrocyte markers and cellular proliferation. For example, the top ontological terms for M2 included "positive regulation of DNA replication" and "purine biosynthetic process." Meanwhile, those of M4 included "glial cell differentiation" and "chromosome segregation." This myelination panel harbored 49 brain-linked CSF markers.

The fourth panel comprised the largest number of modules (M30, M29, M18, M24, and M5), nearly all of which were significantly enriched with microglia and astrocyte markers. Similar to the myelination panel, this fourth panel also contained modules strongly associated with cell proliferation (M30, M29, and M18). Other modules in this group were highly associated with immunological terms, such as "immune effector process" (M5) and "regulation of immune response" (M24). This glial immunity panel contained 42 brain-linked CSF markers. Finally, the last panel included 52 brain-linked markers over four modules (M44, M3, M33, and M38), all of which were ontologically linked to energy storage and metabolism. The largest of these modules (M3) was strongly associated with mitochondria and enriched with neuronal-specific markers. M38, one of the smaller module members of this metabolic panel, also demonstrated modest neuronal specificity.

Overall, these five panels reflected a wide range of cell types and functions in the AD cortex and collectively harbored 271 brain-linked CSF markers (table S2G). To assess the validity of these MS results, we reanalyzed a subset of these 271 biomarkers ($n = 36$) in our discovery CSF samples using a proximity extension assay (PEA), an orthogonal antibody-based technique with multiplexing capacity and high sensitivity and specificity. These 36 targets demonstrated AD fold changes by PEA that strongly correlated with our MS-based findings ($r = 0.87$, $P = 5.6 \times 10^{-12}$), strongly validating the results of our integrative MS analysis (fig. S4).

Synaptic, vascular, and metabolic panels demonstrate divergent expression trends in the brain and CSF

The biological themes highlighted by our five panels, from synaptic signaling to energy metabolism, have all been implicated in the pathogenesis of AD (*1*–*3*). Accordingly, all 15 modules comprising these panels correlated to AD pathology in our discovery brain proteome (Fig. 2B). Most notable were the highly positive pathological correlations among our glial modules and the strongly negative pathological correlations of our largest neuronal modules (M1 and M3). The differential expression analysis of our replication brain proteome (fig. S3D) also highlighted M5- and M18-derived glial proteins among those most increased and M1-associated synaptic proteins among those most decreased in both AsymAD and symptomatic AD. These observations indicated that the 271 CSF markers we had identified among the five panels were linked to disease processes in the AD cortex, including those occurring in early asymptomatic stages.

To better resolve the direction of change of panel proteins in the brain and spinal fluid, we plotted the following for each of the 15 overlapping modules: (i) module abundance levels in the discovery brain dataset and (ii) the differential expression of module proteins in the CSF (fig. S5). Module abundances, or eigenprotein values, in the brain were determined using WGCNA as previously described (*13*). Volcano plots were used to depict the differential expression (AD/control) of module proteins in the CSF. These plots revealed that three of the five panels demonstrated divergent expression trends in the brain and spinal fluid. Both modules of the synaptic panel (M1 and M12) demonstrated decreased abundance levels in the AD brain but overlapped significantly with proteins increased in AD CSF (fig. S5A). The neuronal-associated modules comprising the metabolic panel (M3 and M38) demonstrated similarly discordant brain and CSF expression patterns (fig. S5E). The vascular panel also displayed divergent expression trends, although its modules (M6 and M15) were modestly increased in the AD brain and decreased in diseased CSF (fig. S5B). The two remaining panels comprised large glial networks whose proteins were concordantly up-regulated in both compartments (fig. S5, C and D).

Note that these trends were not universal for all markers within these panels. For instance, the synaptic panel included several proteins significantly decreased in the AD brain and CSF (fig. S5A). Among these down-regulated CSF markers were NPTX2 and VGF of M1, as well as chromogranin B of M12. However, despite these few exceptions, most of our synaptic markers were elevated in the AD spinal fluid. Overall, these analyses were able to distinguish statistically meaningful trends in both the brain and CSF levels for each of our five panels. These trends highlighted complex and often divergent relationships between brain and CSF protein expression in AD.

CSF biomarker panels demonstrate reproducibility and disease specificity

We then narrowed our 271 panel biomarkers to the most promising and reproducible targets using a high-throughput MS replication analysis (CSF replication 1) (Fig. 5A). CSF replication 1 comprised a total of 96 samples derived from the Emory Goizueta ADRC, including control, AsymAD, and AD cohorts (table S1A). These AD cases featured mild cognitive decline (mean MoCA, 20.0 ± 3.8), as well as CSF-confirmed AD biomarker changes (table S1A). In contrast to our discovery CSF analysis, this replication was performed using a more efficient, high-throughput, "single-shot" MS method (no off-line fractionation), comprising a simplified sample preparation protocol without immunodepletion of individual samples. Instead, a single immunodepleted "boost channel" was used to amplify the signals of less abundant proteins (*37*). Although it reduced total proteomic coverage, this single-shot approach markedly decreased machine time and increased the number of TMT-labeled samples that could be feasibly analyzed (*17*, *38*). Overall, this analysis resulted in the identification of 6487 peptides mapping to 1183 protein groups across the 96 cases. As in our discovery CSF analysis, only those proteins quantified in at least 50% of samples were included in subsequent calculations, and the data were regressed for effects of age and sex. This resulted in the final quantification of 792 protein groups, 95% of which were also identified in the discovery CSF dataset.

Since we were specifically interested in validating our 271 brain-linked CSF targets from our integrative analysis, we limited further

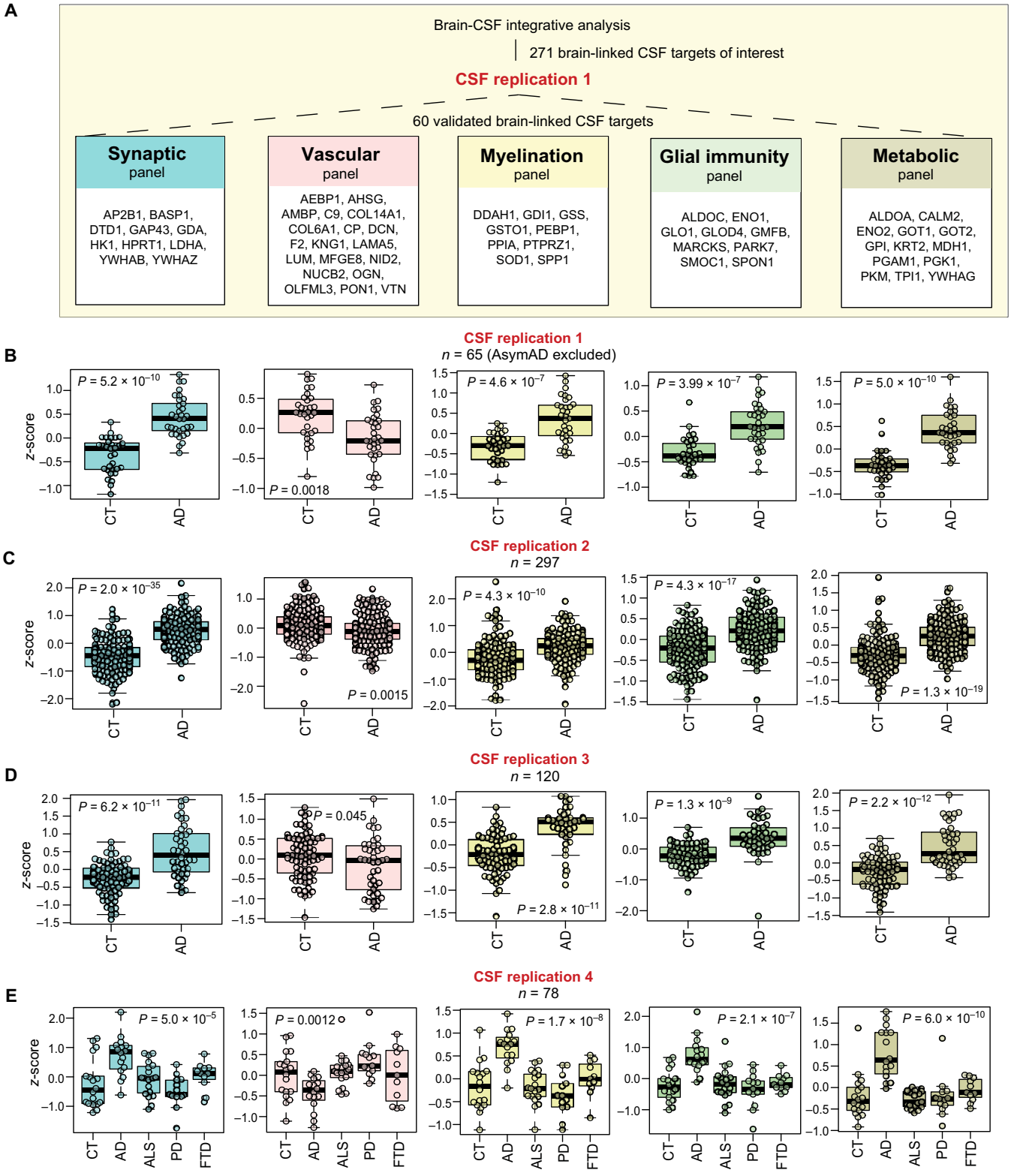

Fig. 5. CSF biomarker panels demonstrate reproducibility and disease specificity in replication cohorts. (**A**) Brain-linked CSF protein targets validated in the first replication CSF cohort and included in the final panels ($n = 60$). (**B** to **E**) Levels of panel biomarkers (composite *z*-score) measured in four CSF replication cohorts. Pairwise *t* test or ANOVA with Tukey post hoc correction was used to assess the statistical significance of abundance changes within each replication analysis. CT, control.

examination of this replication proteome to only these markers. Of these 271 proteins, 100 were detected in CSF replication 1. Figure S6A demonstrates the differential expression of these 100 overlapping markers between the control and AD replication samples. Synaptic and metabolic panel proteins were most increased in AD, while vascular proteins comprised those most decreased in disease. The majority (n = 70) of these 100 overlapping markers maintained the same directionality of change in the two datasets (fig. S6B). These 70 validated brain-linked CSF markers (table S2H) largely reflected previously observed panel expression trends, i.e., down-regulation of vascular proteins and up-regulation of all other panels. Only 10 of these 70 validated proteins demonstrated abundance changes in AD that contradicted these panel trends. To generate panels best reflective of overarching trends in brain and CSF, we excluded these 10 proteins from our final validated panels of interest (Fig. 5A). Therefore, our panels ultimately included a total of 60 proteins validated across two independent CSF AD cohorts analyzed using different sample preparations and MS platforms. z-score expression plots of these final panels across the control and AD cases of CSF replication 1 confirmed the panel trends observed in our discovery CSF cohort (Fig. 5B).

Among these 60 panel proteins were molecules with known connections to AD such as osteopontin (SPP1), a proinflammatory cytokine that has been linked to AD across several studies (*39*–*41*), and GAP43, a synaptic protein with well-characterized links to neurodegeneration (*42*). Among our most strongly validated proteins were markers associated with other neurodegenerative diseases, such as the amyotrophic lateral sclerosis (ALS)–linked superoxide dismutase 1 (SOD1) and parkinsonism associated deglycase (PARK7). We also validated many other markers, such as SMOC1 and brain abundant membrane attached signal protein 1 (BASP1), with limited previous connections to neurodegeneration. Notably, we had difficulty reliably detecting MAPT and certain other AD-associated proteins (e.g., NEFL and NRGN) using this high-throughput single-shot method due to their low overall abundances in the CSF proteome (*43*, *44*).

We then examined these 60 prioritized panel markers in three additional replication analyses. In CSF replication 2, we used single-shot TMT-MS to analyze an independent cohort of 297 control and AD samples from the Emory Goizueta ADRC (*17*). CSF replication 3 comprised a reanalysis of available TMT-MS data from 120 control and patients with AD in Lausanne, Switzerland (*45*). We detected more than two-thirds of our 60 prioritized markers in each of these datasets. Although the Swiss study used a different MS platform and TMT quantification approach (*45*, *46*), we strongly reproduced our panel trends across both replication analyses (Fig. 5, C and D, and table S2, I and J). To assess the disease specificity of our panels, we used TMT-MS to analyze a fourth replication dataset (CSF replication 4) composed of not only control (n = 18) and AD (n = 17) cases but also PD (n = 14), ALS (n = 18), and frontotemporal dementia (FTD) samples (n = 11) (table S1A). We successfully quantified nearly two-thirds of panel proteins (38 of 60) in this cohort. These results highlighted AD-specific changes across all five biomarker panels (Fig. 5E and table S2K). Elevations in the metabolic panel demonstrated the strongest AD specificity, followed closely by the myelination and glial panels. To a lesser degree, FTD demonstrated increases among these panels as well, perhaps reflecting similar underlying network alterations (*17*). In contrast, ALS and PD demonstrated myelination, glial, and metabolic panel profiles nearly identical to those of controls. Overall, despite differences in sample preparation, MS platforms, and TMT quantification approaches, these replication analyses demonstrated highly consistent, AD-specific changes in our prioritized panel markers across >500 unique CSF samples.

CSF biomarker panels reveal heterogeneity among AsymAD cases

The widespread recognition that AD neurodegeneration begins years before the onset of cognitive symptoms has created an urgent need for biomarkers of AsymAD (*5*, *31*). However, increasing evidence suggests that the biology of AsymAD is far from homogeneous and that a complex interplay of risk and resilience contributes to considerable individual variability in the subsequent progression of disease (*47*). While used to identify AsymAD cases, the levels of core CSF biomarkers ($A\beta_{1-42}$, total tau, and p-tau) have still not demonstrated the ability to reliably predict which individuals will progress to dementia (*4*, *7*), indicating that more holistic biomarker tools encompassing multiple aspects of brain-based physiology will likely be required to accurately risk-stratify this population. Thus, we subsequently analyzed our AD-validated biomarker panels in the AsymAD population of CSF replication 1. These 31 AsymAD cases demonstrated abnormal core biomarker levels ($A\beta_{1-42}$/total tau ELISA ratio, <5.5) with intact cognition (mean MoCA, 27.1 ± 2.2) (table S1A). In addition, all individuals with AsymAD had clinical dementia ratings of 0, indicating no evidence of decline in everyday cognitive or functional performance.

We first analyzed the levels of our validated panels across all 96 cases of CSF replication 1, including the AsymAD cohort. We found that several panels featured notable AD-like abundance changes in the AsymAD group, with the vascular panel trending down in AsymAD and all other panels trending upward (Fig. 6A). Accordingly, all panels demonstrated highly significant correlations to ELISA $A\beta_{1-42}$ and total tau levels (Fig. 6B). In contrast, panel correlations to MoCA scores were comparatively less robust. One of the more notable findings of these analyses was the large range of panel abundances within the AsymAD cohort. As shown in Fig. 6A, the panel levels of the AsymAD group often spanned those of both the control and AD cohorts, demonstrating a relatively high degree of variability. To further explore this AsymAD heterogeneity, we applied a multidimensional scaling (MDS) analysis to the 96 cases of CSF replication 1. MDS analysis allows for the visualization of similarities among cases based on certain variables in a dataset. For this clustering analysis, we used the levels of only those validated panel markers with statistically significant alterations ($P < 0.05$, AD/control) in both the CSF discovery and replication 1 proteomes (n = 29) (table S2L). This analysis generated clear spatial clusters between our control and AD cases (Fig. 6C). In contrast, certain AsymAD cases clustered unequivocally among the controls, while others were situated among AD cases. To further explore this AsymAD heterogeneity, we used our MDS plot to define two groups among these AsymAD cases. The first group comprised AsymAD cases that clustered closer to controls (n = 19), while the second featured AsymAD cases with marker profiles closer to AD (n = 12).

We examined the differential protein expression between these control-like and AD-like AsymAD cases (Fig. 6D and table S2L). The resulting volcano plot revealed 14 panel markers significantly altered between these two groups. Most of these markers were members of the synaptic and metabolic panels. However, SOD1 and myristoylated alanine rich protein kinase C substrate (MARCKS),

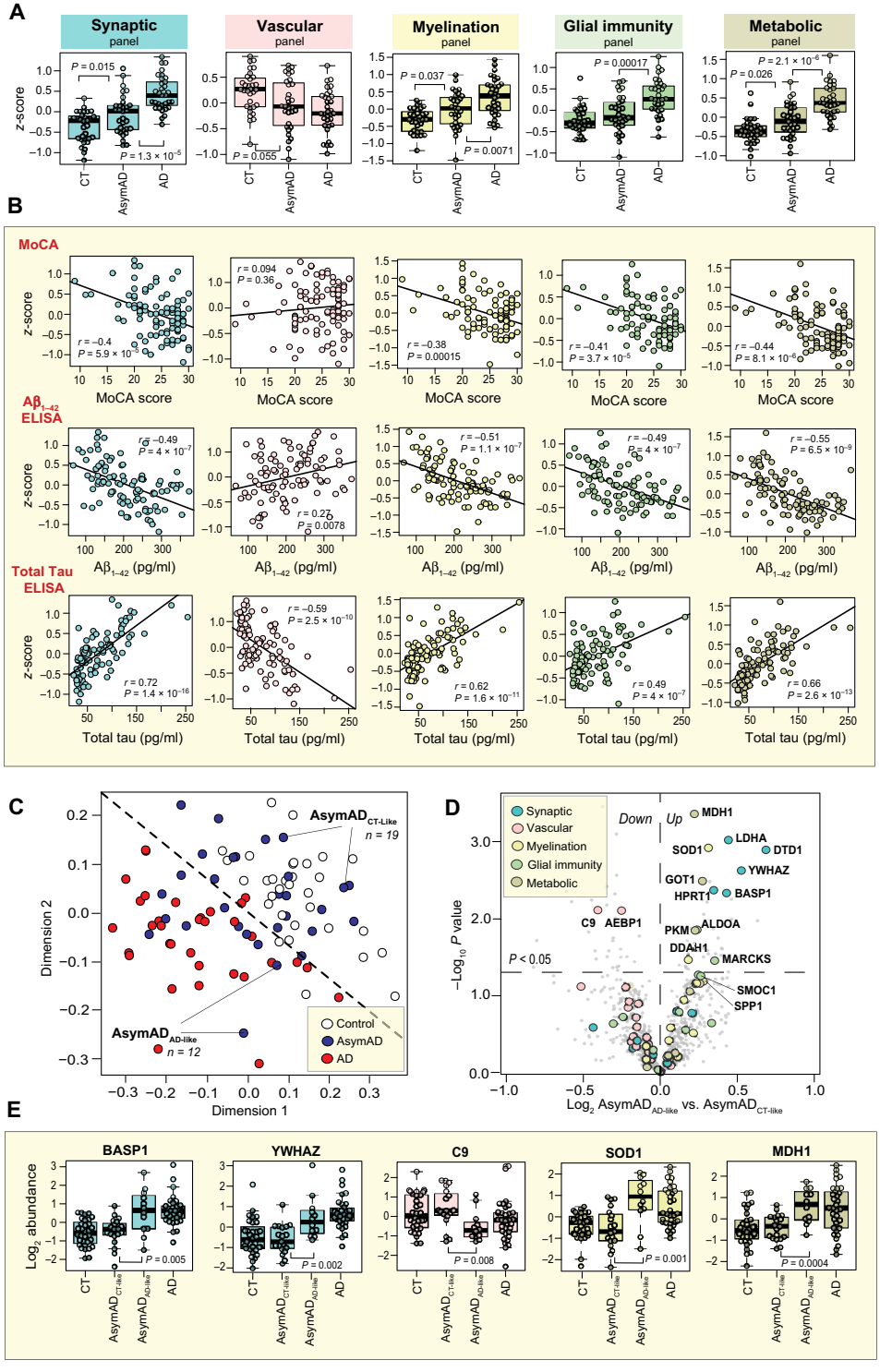

Fig. 6. CSF biomarker panels identify subgroups within AsymAD. (**A**) Expression levels (*z*-score) of CSF biomarker panels across all 96 samples of the CSF replication 1 cohort, including AsymAD. ANOVA with Tukey post hoc correction was used to assess the statistical significance of panel abundance changes. (**B**) Correlation analyses of panel protein abundance levels (*z*-score) to MoCA scores and ELISA $A\beta_{1–42}$ and total tau levels across the CSF replication 1 samples. Pearson correlation coefficients with associated *P* values are shown. (**C**) MDS of the 96 CSF replication 1 cases based on the abundance levels of the 29 validated panel markers that were significantly altered [$P < 0.05$ AD/control (CT)] in both the discovery and CSF replication 1 datasets. This analysis was used to divide the AsymAD group into control-like ($n = 19$) and AD-like ($n = 12$) subgroups. (**D**) Volcano plot displaying the $\log_2$ fold change (*x* axis) against the $-\log_{10}$ statistical *P* value for all CSF replication 1 proteins differentially expressed between the two AsymAD subgroups. Panel biomarkers are colored. (**E**) CSF replication 1 abundance levels of select panel biomarkers differentially expressed between AsymAD subgroups. ANOVA with Tukey post hoc correction was used to assess statistical significance.

members of the myelin and glial immunity panels, respectively, were also among this group (Fig. 6, D and E). The vascular panel also contributed two markers notably decreased in the AD-like AsymAD group, including AE binding protein 1 (AEBP1) and complement family member C9. The control-like and AD-like AsymAD subgroups demonstrated no significant differences in ELISA AB_{1-42} ($P = 0.38$) and p-tau ($P = 0.28$) levels, but did significantly differ in total tau levels ($P = 0.0031$) (fig. S7). There were several panel markers that demonstrated alterations between the two AsymAD subgroups of much greater significance than total tau levels (e.g., YWHAZ, SOD1, and MDH1) (Fig. 6E). Overall, these results indicated that our validated panels may harbor biomarkers capable of subtyping and potentially risk-stratifying individuals with asymptomatic disease.

DISCUSSION

Systems-based biomarker tools are urgently needed to better measure and target the diverse pathophysiology underlying AD. These tools promise to not only transform our diagnostic framework of AD but also propel us toward effective, patient-tailored therapeutic strategies (*1*, *2*). To this end, we applied an unbiased integrative proteomics approach to AD brain and CSF to identify network-based CSF biomarkers reflective of a wide range of brain-based pathophysiology. Our analyses yielded five CSF biomarker panels that (i) reflect synaptic, vascular, myelin, immunological, and metabolic dysfunction; (ii) demonstrate robust reproducibility across varied MS platforms; and (iii) exhibit progressive disease-specific changes throughout early and late AD. Overall, these findings represent a promising step toward the development of a diverse, reliable, network-oriented biomarker tool for AD research and clinical applications.

Our results showcase the highly conserved organization of the AD brain network proteome and support its use as an anchor for systems-based biomarker development. Our analyses demonstrated strong module conservation across two independent TMT-MS datasets comprising both AD and AsymAD brains. These findings expand on our prior work demonstrating strong module preservation across >2000 brain tissues derived from the frontal, parietal, and temporal cortex of multiple independent cohorts (*17*). This consensus network mirrored a variety of the disease-associated changes observed in the current study, including increases in glial-enriched inflammatory modules and decreases in neuronal-enriched modules. As in the current study, this large-scale network also featured significant module changes in AsymAD, showcasing a diverse range of preclinical pathophysiology (*17*).

Nevertheless, within this highly conserved systems-based framework exists more granular biological heterogeneity, particularly among individuals in the earliest stages of AD. Our biomarker panels were able to delineate two subgroups within AsymAD that demonstrated notable differential expression of multiple CSF markers. Our panels were able to highlight biological distinctions among these two subgroups that were not readily apparent among core AD biomarker levels. These AsymAD individuals all featured abnormally low $A\beta_{1-42}$/total tau ratios compared to controls. However, only total tau levels differed significantly between the two AsymAD subgroups, while $A\beta_{1-42}$ and p-tau levels remained relatively comparable. Since high CSF tau appears to predict cognitive symptoms better than $A\beta_{1-42}$ levels (*7*), we suspect that these two AsymAD cohorts may carry different risks of disease progression. Given our limited AsymAD sample size and lack of longitudinal data, further studies are needed to confidently draw these conclusions. However, these results suggest that systems-based CSF panels could enhance our ability to effectively risk-stratify individuals in the asymptomatic stages of disease.

Overall, our findings support a role for a variety of biological functions in AD pathogenesis. However, dysregulated energy metabolism emerged as a prominent theme across all five of our validated marker panels. Metabolic proteins, such as hypoxanthine-guanine phosphoribosyltransferase 1 (HPRT1) and lactate dehydrogenase A (LDHA), were among the most strongly validated synaptic biomarkers, demonstrating highly reproducible increases in AD CSF. Our vascular and glial panels also featured several markers involved in the metabolism of oxidative species. These findings align with the critical role that metabolic processes play throughout the brain to meet the high energy demands of not only neurons but also astrocytes and other glial cells (*17*, *48*). Our results support the growing evidence that altered redox potential and disrupted energy pathways may comprise the central link between several key processes implicated in AD pathogenesis, including mitochondrial dysregulation, glial-mediated inflammation, and vascular damage (*49*). Furthermore, metabolic CSF biomarkers comprised the bulk of differentially abundant proteins between our control-like and AD-like AsymAD subgroups, suggesting that these disruptions of energy and redox pathways may be critical during preclinical stages of disease.

The divergent brain and CSF panel trends we observed also have intriguing biological implications. The neuron-enriched synaptic and metabolic panels demonstrated decreased levels in the AD brain and increased abundance in CSF. Given that neurons are enriched with energy-generating mitochondria at synapses to fuel their numerous specialized signals (*50*), the similarities in the expression profiles of these two neuronal panels are expected. Neuronal loss and the extrusion of damaged cells could account for these brain and CSF panel trends in later disease but do not explain the early panel changes we observed (*13*). One possible explanation for these findings in early, asymptomatic disease is aberrant synaptic pruning. Emerging evidence in mouse models has suggested that microglial-mediated synaptic phagocytosis may be aberrantly activated in AD and account for early synaptic loss in the brain (*51*). This discarded synaptic material may then accumulate in CSF, accounting for the CSF increases we observed in our neuronal panels. Immune-mediated synaptic pruning may also partially account for the elevations of glial proteins we observed in both the brain and CSF throughout the course of disease. Aside from synaptic pruning, global abnormalities in exocytic pathways may also result in the divergent brain and CSF expression of neuronal markers. Multiple studies have demonstrated altered exosome content in AD brain pathogenesis (*52*). Exocytic pathways have also been linked to Aβ propagation (*53*, *54*). Notably, the inhibition of exosome secretion may reduce AD-like pathology in a transgenic mouse model of AD (*55*).

Meanwhile, proteins in the vascular panel demonstrated modest increases in the AD brain but stark decreases in CSF. Blood-brain barrier (BBB) dysfunction could partially explain these findings. BBB breakdown in AD has been demonstrated by numerous independent postmortem human studies (*56*, *57*). These investigations have confirmed a variety of aberrant activity surrounding this tightly sealed layer of endothelial cells, including brain capillary leakages and the perivascular accumulation of blood-derived proteins (*57*). This could provide a simple explanation for elevated vascular

proteins in the brain but fails to entirely account for depletion of these same proteins in CSF. One possibility is that the central nervous system is actively sequestering these molecules to address heightened levels of inflammation and oxidative stress. Several of the most decreased CSF proteins within this panel, particularly those involved in lipoprotein regulation, have been implicated in neuroprotective processes that suppress harmful levels of inflammation and reactive oxygen species. This is certainly true of paroxonase 1 (PON1), a lipoprotein-binding enzyme responsible for reducing oxidative stress levels in the circulation (*58*, *59*). Alpha-1-microglobulin/bikunin precursor (AMBP), another significantly down-regulated vascular panel marker, serves as a precursor for the lipid transporter, bikunin, which has also been implicated in inflammation suppression and neuroprotection (*60*, *61*).

Despite fueling a variety of interesting hypotheses, the inability to directly probe biochemical disease mechanisms is a well-known limitation of discovery-driven proteomic analysis. Thus, further studies are necessary to confidently define the mechanisms underlying these biomarker panels. To progress toward clinical MS-based assay development, future directions will also require large-scale biomarker validation using targeted quantitation methods, such as selective or parallel reaction monitoring (*62*). We recently validated many of the CSF protein changes described here using parallel reaction monitoring (*63*). Several prioritized panel targets were quantified with marked precision, including YWHAZ, ALDOA, and SMOC1, which map to our synaptic, metabolic, and inflammatory panels, respectively (*63*). Data-independent acquisition (DIA) and other MS-based strategies may also prove useful for target validation. Bader *et al.* (*64*) recently demonstrated significant overlap between the AD biomarkers identified in our CSF discovery dataset and an independent DIA-MS dataset composed of nearly 200 CSF samples across three different European cohorts. These recent studies support the translational potential of our panels into reliable MS-based assays. Traditional antibody- and aptamer-based assays will also be important to further develop key AD biomarkers that, due to low CSF abundance, are more difficult to detect using high-throughput MS methods. NEFL and NRGN are two such examples of low-abundant CSF biomarkers that mapped to panels in our integrative analysis but could not be reliably detected using our single-shot MS strategy. Multiplex antibody-based targeting strategies, such as PEA, may facilitate clinical translation of these markers.

Overall, this study offers a unique proteomic approach for the identification and validation of diverse systems-based CSF AD biomarkers. The optimization of these marker panels across additional AD cohorts and MS platforms could prove promising for the advancement of AD risk stratification and therapeutics. Studies assessing the longitudinal levels of these panels over time will also be critical to determine which combination of markers best stratify risk in early disease and change in accordance to disease severity.

MATERIALS AND METHODS

CSF samples

Except for the CSF replication 3 samples, all CSF samples used in this study were collected under the auspices of the Emory ADRC or closely affiliated research institutions. In total, there were four cohorts of Emory CSF samples used in these proteomics studies. The discovery CSF cohort contained samples from 20 healthy controls and 20 patients with AD. CSF replication 1 included samples from 32 healthy controls, 31 individuals with AsymAD, and 33 individuals with AD. CSF replication 2 contained 147 control and 150 AD samples. The multidisease CSF replication 4 cohort comprised 18 control, 17 AD, 19 ALS, 13 PD, and 11 FTD samples. All Emory research participants were provided informed consent under protocols approved by the Institutional Review Board at Emory University. CSF was collected by lumbar puncture and banked according to the 2014 National Institute on Aging best practice guidelines for Alzheimer's Disease Centers (https://alz.washington.edu/BiospecimenTaskForce.html). Control and patients with AsymAD and AD received standardized cognitive assessments in the Emory Cognitive Neurology Clinic or Goizueta ADRC and their CSF samples subjected to ELISA $A\beta_{1-42}$, total tau, and p-tau analysis by the INNO-BIA AlzBio3 Luminex Assay (*65*). The ELISA values were used to support subject diagnostic classifications based on established AD biomarker cutoff criteria (*66*, *67*). Basic demographic and diagnostic data for other CSF diagnoses (FTD, ALS, and PD) were also obtained from the Emory ADRC or affiliated research institutions. Summarized case metadata for these Emory CSF cases can be found in table S1A. Characteristics of the Swiss CSF replication 3 cohort were previously published (*45*).

Protein digestion of CSF

CSF discovery samples

To increase the depth of our discovery CSF dataset, immunodepletion of highly abundant proteins was performed before trypsin digestion. Briefly, 130 µl of CSF from each of the 40 individual CSF samples was incubated with equal volume (130 µl) of High Select Top14 Abundant Protein Depletion Resin (Thermo Fisher Scientific, A36372) at room temperature in centrifuge columns (Thermo Fisher Scientific, A89868). After 15 min of rotation, the samples were centrifuged at 1000*g* for 2 min. Sample flow-through was concentrated with a 3K Ultra Centrifugal Filter Device (Millipore, UFC500396) by centrifugation at 14,000*g* for 30 min. All sample volumes were diluted to 75 µl with phosphate-buffered saline. Protein concentration was assessed by bicinchoninic acid (BCA) method according to the manufacturer's protocol (Thermo Fisher Scientific). Immunodepleted CSF (60 µl) from all 40 samples was digested with lysyl endopeptidase (LysC) and trypsin. Briefly, the samples were reduced and alkylated with 1.2 µl of 0.5 M tris-2(-carboxyethyl)-phosphine and 3 µl of 0.8 M chloroacetamide at 90°C for 10 min, followed by water bath sonication for 15 min. Samples were diluted with 193 µl of 8 M urea buffer [8 M urea and 100 mM $NaHPO_4$ (pH 8.5)] to a final concentration of 6 M urea. LysC (4.5 µg; Wako) was used for overnight digestion at room temperature. Samples were then diluted to 1 M urea with 50 mM ammonium bicarbonate (ABC) (*68*). An equal amount (4.5 µg) of trypsin (Promega) was added, and the samples were subsequently incubated for 12 hours. The digested peptide solutions were acidified to a final concentration of 1% formic acid (FA) and 0.1% trifluoroacetic acid (TFA) (*66*), followed by desalting with 50 mg of Sep-Pak C18 columns (Waters) as described previously (*25*). The peptides were subsequently eluted in 1 ml of 50% acetonitrile (ACN). To normalize protein quantification across batches (*25*), 100 µl of aliquots from all 40 CSF samples were combined to generate a pooled sample, which was then divided into five global internal standard (GIS) (*48*) samples. All individual samples and the pooled standards were dried by speed vacuum (Labconco).

CSF replication samples

Immunodepletion and digestion of CSF replication 3 samples have been previously described by Dayon and colleagues (*45*, *46*). The

remaining replication samples were not individually immunodepleted. These nondepleted samples were digested in trypsin as previously described (*17*). For each replication analysis, 120 µl of aliquots of eluted peptides from each sample were pooled together and split into equal volume aliquots for use as the global internal standard (*48*) for TMT labeling. All individual samples and the pooled standard were dried by speed vacuum (Labconco). To boost the signal of low abundance CSF proteins, a "boost" sample [i.e., a biological sample mimicking study samples but accessible in a much larger quantity (*37*, *69*)] was prepared for each replication analysis by combining 125 µl from each sample into one pooled CSF sample (*17*). This pooled sample was subsequently immunodepleted using 12 ml of High Select Top14 Abundant Protein Depletion Resin (Thermo Fisher Scientific, A36372), digested as described above, and included in subsequent multiplex TMT labeling.

TMT labeling of CSF

CSF discovery samples

All 40 samples and 5 GIS samples were divided into five batches, labeled using an 11-plex TMT kit (Thermo Fisher Scientific, A34808, lot no. for TMT 10-plex: SI258088, 131C channel SJ258847), and derivatized as previously described (*25*). See the "Data and materials availability" section for sample to batch arrangement. Nine of the 11 TMT channels were used for labeling: 127N, 128N, 128C, 129N, 129C, 130N, 130C, 131N, and 131C. Briefly, 5 mg of each TMT reagent was dissolved in 256 µl of anhydrous ACN. Each CSF peptide digest was resuspended in 50 µl of 100 mM triethylammonium bicarbonate (TEAB) buffer, and 20.5 µl of TMT reagent solution was subsequently added. After 1 hour, the reaction was quenched with 4 µl of 5% hydroxylamine (Thermo Fisher Scientific, 90115) for 15 min. After labeling, the peptide solutions were combined according to the batch arrangement. Each TMT batch was desalted with 100 mg of Sep-Pak C18 columns (Waters) and dried by speed vacuum (Labconco).

CSF replication samples

TMT labeling of CSF replication 3 samples has been previously described by Dayon and colleagues (*45*, *46*). Multiplex TMT labeling of the remaining replication samples was performed as previously described (*17*). For each replication analysis, all CSF samples, including the GIS and boost samples, were labeled using an 11-plex (CSF replications 1 and 2) or 16-plex (CSF replication 4) TMT kit (Thermo Fisher Scientific) (*70*). See the "Data and materials availability" section for sample to batch arrangement. One channel was dedicated to the boost sample in each plex. The immunodepleted boost sample was dissolved in 1.25 ml of 100 mM TEAB and labeled with 2 × 5 mg of reagent. In each batch, the pooled boost channel was equivalent to 50-fold volume of each of the CSF samples. After labeling, the peptide solutions were combined according to the batch arrangement. Each TMT batch was then desalted with 100 mg of Sep-Pak C18 columns (Waters) and dried by speed vacuum (Labconco).

High-pH fractionation of CSF

To enhance the depth of the discovery CSF proteome, these samples were subjected to high-pH fractionation as previously described (*71*). TMT-labeled peptides (160 µg) from each discovery sample were dissolved in 100 µl of loading buffer [1 mM ammonium formate in 2% (v/v) ACN], injected completely with an autosampler, and fractionated using a ZORBAX 300Extend-C18 column (2.1 mm by 150 mm, 3.5 µm; Agilent Technologies) on an Agilent 1100 HPLC (high-performance liquid chromatography) system monitored at 280 nm. A total of 96 fractions were collected over a 60-min gradient of 100% mobile phase A [4.5 mM ammonium formate (pH 10) in 2% (v/v) ACN] from 0 to 2 min, 0 to 12% mobile phase B [4.5 mM ammonium formate (pH 10) in 90% (v/v) ACN] from 2 to 8 min, 12 to 40% mobile phase B from 8 to 36 min, 40 to 44% mobile phase B from 36 to 40 min, 44 to 60% mobile phase B from 40 to 45 min, and 60% mobile phase B until completion with a flow rate of 0.4 ml/min. The 96 fractions were collected with an even time distribution and pooled into 30 fractions.

MS analysis and data acquisition of CSF

CSF discovery samples

Discovery CSF samples were analyzed by MS/MS and the data acquired from MS2 scans. An equal volume of each high-pH peptide fraction was first resuspended in loading buffer (0.1% FA, 0.03% TFA, and 1% ACN). Using an EASY-nanoLC system, peptide eluents were separated on a C18 25-cm-long 75-µM internal diameter (ID) fused silica column (New Objective, Woburn, MA) packed in-house with a 1.9-µm ReproSil-Pur C18-AQ resin (Maisch, Germany). Elution was performed over a 120-min gradient at a rate of 225 nl/min with buffer B ranging from 1 to 90% (buffer A, 0.1% FA in water; buffer B, 0.1% FA in ACN). An Orbitrap HF-X mass spectrometer (Thermo Fisher Scientific) was set to acquire data in positive ion mode using data-dependent acquisition. Each cycle consisted of one full MS scan, followed by a maximum of 10 MS/MS scans. Full MS scans were collected at a resolution of 120,000 [400 to 1600 mass/charge ratio (m/z) range, 3×10^6 automatic gain control (AGC) target, and 100-ms maximum ion injection time]. All higher-energy collision-induced dissociation (HCD) MS/MS spectra were acquired at a resolution of 45,000 (1.6 m/z isolation width, 35% collision energy, 1×10^5 AGC target, and 86-ms maximum ion time). Dynamic exclusion was set to exclude previously sequenced peaks for 20 s within a 10-ppm (parts per million) isolation window. See the "Data and materials availability" section for all raw MS files and matched peptides.

CSF replication samples

MS analysis of CSF replication 3 samples has been previously described by Dayon and colleagues (*45*, *46*). The remaining CSF replication samples were analyzed by single-shot TMT-MS with MS3-based data acquisition on an Orbitrap Fusion Lumos mass spectrometer (Thermo Fisher Scientific) interfaced with high-field asymmetric waveform ion mobility spectrometry (FAIMS), as previously described (*17*). When combined with synchronous precursor selection MS3-based quantitation (SPS-MS3), this FAIMS-based strategy is especially useful for enhancing accuracy of protein quantification in samples with high dynamic ranges of protein abundance, such as albumin- and immunoglobulin-rich CSF (*38*). Accordingly, we found that the use of FAIMS Pro with SPS-MS3 reduced the interference of peptide co-isolation and, in turn, increased the number of proteins identified in our CSF dataset by approximately 30% (fig. S8, A to E). Independent of FAIMS, the use of an immunodepleted boost channel in our single-shot TMT-MS approach also increased CSF protein detection by nearly 40%, directly promoting the identification of several key AD biomarkers (fig. S8F). See the "Data and materials availability" section for all raw MS files. TMT-MS analysis of the Swiss CSF replication 3 cohort has been described (*45*, *46*), and raw files were downloaded from ProteomeXchange, resource PXD009589.

Postmortem brain tissues

All brain tissues used in this study were derived from the DLPFC and processed in the Emory Goizueta ADRC. Postmortem neuropathological evaluation of amyloid plaque distribution was performed according to CERAD criteria (*72*), while the extent of neurofibrillary tangle pathology was assessed in accordance with the Braak staging system (*73*). All AD cases met NIA-Reagan criteria for the diagnosis of AD (high likelihood) (*74*). PD cases also met established criteria and guidelines for diagnosis (*75*). Cases were classified as comorbid AD and PD (AD/PD) when they met pathological criteria for amyloid plaque, neurofibrillary tangle, and Lewy body burden. Pathological and clinical evaluations for the AsymAD brain tissues have been previously described (*13*). Two cohorts of brain tissues were used in the proteomic studies. The discovery brain cohort included tissues from 10 healthy control, 10 PD, 10 AD/PD, and 10 AD cases. The replication brain cohort included 19 cases identical to the discovery cohort (10 control and 9 AD cases), as well as 8 AsymAD cases unique to this cohort. Summarized case metadata, including disease state, gender, race, apolipoprotein genotype, age of death, Mini-Mental State Examination and PMI, are provided in table S1B.

Protein digestion of brain tissue

Tissue homogenization for both the discovery and replication brain samples was performed as previously reported (*25*). BCA was then used to determine the protein concentration for each sample before subsequent digestion. Approximately 100 μg of protein was digested for each discovery brain sample, while 500 μg of protein was digested for each replication sample. Just before digestion, all samples were reduced with 1 mM dithiothreitol at room temperature for 30 min and alkylated with 5 mM iodoacetamide in the dark for another 30 min. LysC (Wako) at 1:100 (w/w) was then added to each sample, and digestion was performed overnight. Samples were then diluted sevenfold with 50 mM ABC. Trypsin (Promega) was then added at 1:50 (w/w), and digestion was continued for another 12 to 16 hours. Each peptide solution was acidified to a final concentration of 1% (v/v) FA and 0.1% (v/v) TFA. The discovery brain samples were desalted with 100 mg of Sep-Pak C18 columns (Waters) and eluted in 1 ml of 50% (v/v) ACN as described previously (*25*). A 200-μl aliquot was removed from each discovery sample and combined to generate a pooled sample, which was subsequently divided into 10 GIS samples. Because a greater amount of protein was digested in the replication analysis, each sample was desalted with a 200-g Sep-Pak column and eluted in 3 ml of 50% (v/v) ACN. A 600-μl aliquot was removed from each replication sample and combined to generate a pooled sample, which was then divided into six GIS samples. All digested peptide solutions from both the discovery and replication brain cohorts were dried by speed vacuum.

TMT labeling of brain tissue

TMT labeling of discovery brain tissues was performed using 10-plex reagents as previously described (*25*). In similar fashion, the 27 individual and 6 GIS samples of the replication brain cohort were randomized into three batches and labeled using 11-plex TMT reagents. See the "Data and materials availability" section for sample to batch arrangement. All 11 TMT channels were used for labeling. TMT reagent (5 mg) was dissolved in 56 μl of anhydrous ACN. Each peptide solution was then reconstituted in 400 μl of 100 mM TEAB buffer, and 164 μl (3.2 mg) of labeling reagent was subsequently added. After 1 hour, the reaction was quenched with 32 μl of 5% hydroxylamine. After labeling, the peptide solutions were combined according to the batch arrangement. Each TMT batch was then desalted with 500 mg of Sep-Pak C18 columns (Waters), and eluted peptides were dried by speed vacuum (Labconco).

Fractionation of brain tissue

All TMT-labeled samples of the discovery brain cohort were subjected to electrostatic repulsion-hydrophilic interaction chromatography fractionation before proteomic analysis as previously reported (*25*). In contrast, the replication brain samples were separated via high-pH fractionation. For each replication sample, approximately 4 mg of TMT-labeled peptides were resuspended in 850 μl of loading buffer [1 mM ammonium formate in 2% (v/v) ACN], injected completely with an autosampler, and fractionated using a ZORBAX 300Extend-C18 column (4.6 mm by 250 mm, 5 μm; Agilent Technologies) on an Agilent 1100 HPLC system monitored at 280 nm. A total of 96 fractions were collected over a 96-min gradient of 100% mobile phase A [4.5 mM ammonium formate (pH 10) in 2% (v/v) ACN] from 0 to 7 min, 0 to 16% mobile phase B [4.5 mM ammonium formate (pH 10) in 90% (v/v) ACN] from 7 to 13 min, 16 to 40% mobile phase B from 13 to 73 min, 40 to 44% mobile phase B from 73 to 77 min, 44 to 60% mobile phase B from 77 to 82 min, and 60% mobile phase B until completion with a flow rate of 0.8 ml/min. The 96 fractions were collected with an even time distribution and pooled into 24 fractions.

MS analysis and data acquisition of brain tissue

MS procedures and MS3-based data acquisition of the discovery brain samples have been previously reported (*25*). In contrast to the discovery brain tissues, replication samples were analyzed by MS/MS and the data acquired from MS2 scans. Briefly, an equal volume of each high-pH peptide replication fraction was first resuspended in loading buffer (0.1% FA, 0.03% TFA, and 1% ACN). Using an EASY-nanoLC system, peptide eluents were then separated on a C18 25-cm-long 75 μM ID fused silica column (New Objective, Woburn, MA) packed in-house with a 1.9-μm Reprosil-Pur C18-AQ resin (Maisch, Germany). Elution was performed over a 140-min gradient at a rate of 225 nl/min with buffer B ranging from 1 to 90% (buffer A, 0.1% FA in water; buffer B, 80% ACN in water and 0.1% FA). An Orbitrap Fusion mass spectrometer (Thermo Fisher Scientific) was set to acquire data in top speed mode with 3-s cycles. Full MS scans were collected at a resolution of 120,000 (375 to 1500 m/z range, 4×10^5 AGC target, and 50-ms maximum ion time). All HCD MS/MS spectra were acquired at a resolution of 50,000 (0.7 m/z isolation width, 38% collision energy, 1×10^5 AGC target, and 105-ms maximum ion time). Dynamic exclusion was set to exclude previously sequenced peaks for 20 s within a 10-ppm isolation window. Only charge states from 2+ to 7+ were chosen for MS/MS. See the "Data and materials availability" section for all raw MS files and matched peptides.

Database search and protein quantification

All raw brain and CSF files were analyzed using the Proteome Discoverer Suite version 2.1 (Thermo Fisher Scientific), with the exception of the CSF replication datasets, which were analyzed using version 2.3 (*17*). MS/MS spectra were searched against the UniProtKB human proteome database (downloaded April 2015 with 90,411 total sequences). The SEQUEST HT search engine was used with the following parameters: fully tryptic specificity; maximum of two missed cleavages; minimum peptide length of 6; fixed modifications for

TMT tags on lysine residues and peptide N termini (+229.162932 Da) and carbamidomethylation of cysteine residues (+57.02146 Da); variable modifications for oxidation of methionine residues (+15.99492 Da) and deamidation of asparagine and glutamine (+0.984 Da); precursor mass tolerance of 20 ppm; and fragment mass tolerance of either 0.05 Da (MS2 data) or 0.6 Da (MS3 data). The Percolator node was used to filter peptide spectral matches to an FDR of less than 1% using a target decoy strategy. Following spectral assignment, peptides were assembled into proteins and were further filtered on the basis of the combined probabilities of their constituent peptides to a final FDR of 1%. In cases of redundancy, shared peptides were assigned to the protein sequence in adherence with the principles of parsimony. Reporter ions were quantified from MS3 or MS2 scans using an integration tolerance of 20 ppm with the most confident centroid setting, as previously described (*17*, *25*).

Adjustment for batch and other sources of variance

For all datasets, only those proteins quantified in ≥50% of samples were included in subsequent analyses. All data were also subjected to iterative outlier removal, as previously described (*13*, *17*). In the discovery CSF analysis, one severe outlier was detected and therefore removed from all subsequent analyses. In contrast, no outliers were found among the replication CSF cohorts. This algorithm also failed to detect outliers among the brain datasets, even with the fold SD cutoff set more stringently to 2.5. For the CSF cohorts, batch correction was performed using a median polish algorithm for removing technical variance, as previously described (*17*). The brain datasets were not subjected to this batch correction, although their protein abundance values were normalized by the GIS within each batch. Bootstrap regression for age at death, sex, and PMI (in the case of brain tissues) was performed on the protein $\log_2$ abundance ratios of all cohorts, excepting CSF replication 3 for which age and sex were not provided because of European confidentiality guidelines (*45*). A principal components analysis of the expression data confirmed appropriate regression of selected traits.

Differential expression analysis

Pairwise differentially expressed proteins were identified using Student's *t* test, followed by Benjamini-Hochberg (BH) FDR correction. Differential expression across three or more groups was performed using a one-way ANOVA, followed by Tukey's post hoc test. Differential expression was presented in volcano plots, which were generated with the ggplot2 package in R v3.5.2.

Weighted gene correlation network analysis

Discovery brain proteome

As previously described (*13*), a weighted protein coexpression network of the discovery brain dataset was derived from the post-regressed protein abundance values using the blockwiseModules WGCNA function (WGCNA 1.66 R package) with the following settings: soft threshold power beta = 7.5, deepSplit = 4, minimum module size = 25, merge cut height = 0.12, signed network with partitioning about medoids respecting the dendrogram, TOMDenominator = "mean," and a reassignment threshold of $P < 0.05$. Module eigenproteins were defined as previously described (*13*), each representing the largest principle component of all proteins within the module. Pearson correlations between module eigenproteins and each quantified protein in the dataset were used to assign a measure of intramodule membership (i.e., kME) to each protein. Module eigenproteins were also correlated with AD diagnosis and levels of amyloid and tau burden using biweight midcorrelation analysis.

Transcriptome

The R package WGCNA was used to construct a coexpression network on transcriptomic data downloaded from Gene Expression Omnibus (#GSE33000) (*76*). The WGCNA algorithm settings for this analysis have been previously described (*13*). The resulting 20 modules were used to calculate module eigengenes, which were subsequently correlated with different disease traits.

GO and cell type enrichment analyses

To characterize modules of proteins based on GO annotation, we used GO Elite v1.2.5 (*77*) with pruned output Fisher's exact overrepresentation *z*-scores visualized using an in-house R script, as previously described (*13*). The background proteome consisted of all proteins in each specific dataset. As outlined previously (*13*), cell type enrichment for each of the modules was performed by cross-referencing the corresponding gene symbols of each module with cell type–specific gene lists derived from previously published RNA-seq data (*29*). Significance of cell type enrichment within each module was then determined using a one-tailed FET and corrected for multiple comparisons by the BH FDR method.

Module preservation analysis

To assess preservation of the discovery brain modules in the replication brain proteome, a coexpression network was built for the replication dataset using similar WGCNA parameters with only slight modifications: soft threshold beta = 15, deepSplit = 3, and merge cut height = 0.25. Preservation of the discovery brain modules in this replication network was then tested using the R WGCNA::modulePreservation function with 500 permutations, as previously described (*13*).

Overrepresentation analysis of RNA and protein networks

Gene set enrichment for the overrepresentation analysis of the brain proteome and transcriptome networks was performed using a one-sided FET with 95% confidence intervals. To reduce false positives, FDR-adjusted *P* values were used for multiple hypergeometric test comparisons, and those corrected $P < 0.05$ were considered significant. The background for this overrepresentation analysis comprised frontal cortex expression levels from array data.

Integrative analysis of brain and CSF proteomic datasets

Quantified proteins of the discovery CSF dataset were assessed for overrepresentation in discovery brain modules using a hypergeometric FET, and those modules with BH-corrected $P < 0.05$ were considered significant. In similar fashion, separate FET analyses were performed to identify modules with significant overlap among differentially expressed CSF proteins, including those significantly up-regulated or down-regulated in AD compared to controls [P(AD/control) < 0.05]. The 15 modules with meaningful levels of CSF overlap from these three FET analyses were included in the five biomarker panels that were subsequently validated in the CSF replication experiments. The expression trends of the validated panels of interest were examined in each replication cohort by calculating composite *z*-scores of protein levels across disease states. Kruskal-Wallis nonparametric ANOVA or pairwise *t*-test was performed on these *z*-scores to assess for significant differences.

Olink proteomic analysis

CSF aliquots from a subset of cases in our discovery CSF cohort were sent to Olink Proteomics (Uppsala, Sweden) for analysis using all human assays available at the time of this study (1196 proteins). All samples passed quality control measures, were randomized per Olink protocol, and run on a single plate. Results were reported as Normalized Protein eXpression (NPX) values in $\log_2$ scale for relative quantification of protein levels across samples. We then median-centered these NPX data in R v3.5.2. Outliers were detected using WGCNA-based Z.K connectivity (>3 SD), resulting in the removal of one sample. The relative abundance data were regressed for age and sex covariance. These post-regressed data were then used to calculate protein fold changes between control and AD samples, which were subsequently correlated to the discovery TMT-MS data.

MDS analysis

The MDS analysis of CSF replication 1 was performed using the limma package of R statistical software. A linear equation was selected to elicit a line across that the MDS plot separating control cases from those with AD. This line also divided the AsymAD cases into control-like and AD-like subgroups. All proteins measured in these AsymAD samples were then subjected to a *t* test comparing their abundance levels in these subclasses of AsymAD.

Western blotting

Equal amounts of each sample (10 or 20 μg) were boiled in Laemmli sample buffer [8% glycerol, 2% SDS, 50 mM tris (pH 6.8), and 3.25% β-mercaptoethanol] for 10 min and resolved by SDS–polyacrylamide gel electrophoresis on Bolt 4 to 12% bis-tris gels (Thermo Fisher Scientific). Gels were then transferred onto nitrocellulose membranes, which were blocked in SuperBlock blocking buffer (Thermo Fisher Scientific) for 30 min at room temperature and probed with primary antibody overnight at 4°C. Membranes were then incubated with fluorophore-conjugated secondary antibodies (1:10,000) for 1 hour at room temperature. Images were captured using an Odyssey Infrared Imaging System (LI-COR Biosciences). Primary antibodies used in this study included glyceraldehyde-3-phosphate dehydrogenase (1:2000; mouse monoclonal, Abcam, ab8245), SFRP1 (1:500; rabbit monoclonal, Abcam, ab126613), MDK (1:1000: rabbit monoclonal, Abcam, ab52637), CD44 (1:1000; rabbit polyclonal, ab157107), and VGF (1:500; rabbit polyclonal, ab69989).

SUPPLEMENTARY MATERIALS

Supplementary material for this article is available at http://advances.sciencemag.org/cgi/content/full/6/43/eaaz9360/DC1

View/request a protocol for this paper from *Bio-protocol*.

REFERENCES AND NOTES

1. S. Lista, H. Zetterberg, S. E. O'Bryant, K. Blennow, H. Hampel, Evolving relevance of neuroproteomics in Alzheimer's disease. *Methods Mol. Biol.* **1598**, 101–115 (2017).
2. J. I. Castrillo, S. Lista, H. Hampel, C. W. Ritchie, Systems biology methods for Alzheimer's disease research toward molecular signatures, subtypes, and stages and precision medicine: Application in cohort studies and trials. *Methods Mol. Biol.* **1750**, 31–66 (2018).
3. B. De Strooper, E. Karran, The cellular phase of Alzheimer's disease. *Cell* **164**, 603–615 (2016).
4. K. Blennow, H. Hampel, M. Weiner, H. Zetterberg, Cerebrospinal fluid and plasma biomarkers in Alzheimer disease. *Nat. Rev. Neurol.* **6**, 131–144 (2010).
5. C. R. Jack Jr., D. A. Bennett, K. Blennow, M. C. Carrillo, B. Dunn, S. B. Haeberlein, D. M. Holtzman, W. Jagust, F. Jessen, J. Karlawish, E. Liu, J. L. Molinuevo, T. Montine, C. Phelps, K. P. Rankin, C. C. Rowe, P. Scheltens, E. Siemers, H. M. Snyder, R. Sperling, NIA-AA research framework: Toward a biological definition of Alzheimer's disease. *Alzheimers Dement.* **14**, 535–562 (2018).
6. B. Olsson, R. Lautner, U. Andreasson, A. Öhrfelt, E. Portelius, M. Bjerke, M. Hölttä, C. Rosén, C. Olsson, G. Strobel, E. Wu, K. Dakin, M. Petzold, K. Blennow, H. Zetterberg, CSF and blood biomarkers for the diagnosis of Alzheimer's disease: A systematic review and meta-analysis. *Lancet Neurol.* **15**, 673–684 (2016).
7. K. Blennow, H. Zetterberg, Biomarkers for Alzheimer's disease: Current status and prospects for the future. *J. Intern. Med.* **284**, 643–663 (2018).
8. R. A. Armstrong, P. L. Lantos, N. J. Cairns, Overlap between neurodegenerative disorders. *Neuropathology* **25**, 111–124 (2005).
9. A. Kapasi, C. DeCarli, J. A. Schneider, Impact of multiple pathologies on the threshold for clinically overt dementia. *Acta Neuropathol.* **134**, 171–186 (2017).
10. R. J. Hodes, N. Buckholtz, Accelerating Medicines Partnership: Alzheimer's disease (AMP-AD) knowledge portal aids Alzheimer's drug discovery through open data sharing. *Expert Opin. Ther. Targets* **20**, 389–391 (2016).
11. P. Langfelder, S. Horvath, WGCNA: An R package for weighted correlation network analysis. *BMC Bioinformatics* **9**, 559 (2008).
12. N. N. Parikshak, M. J. Gandal, D. H. Geschwind, Systems biology and gene networks in neurodevelopmental and neurodegenerative disorders. *Nat. Rev. Genet.* **16**, 441–458 (2015).
13. N. T. Seyfried, E. B. Dammer, V. Swarup, D. Nandakumar, D. M. Duong, L. Yin, Q. Deng, T. Nguyen, C. M. Hales, T. Wingo, J. Glass, M. Gearing, M. Thambisetty, J. C. Troncoso, D. H. Geschwind, J. J. Lah, A. I. Levey, A multi-network approach identifies protein-specific co-expression in asymptomatic and symptomatic Alzheimer's disease. *Cell Syst.* **4**, 60–72.e4 (2017).
14. J. Dai, E. C. B. Johnson, E. B. Dammer, D. M. Duong, M. Gearing, J. J. Lah, A. I. Levey, T. S. Wingo, N. T. Seyfried, Effects of *APOE* genotype on brain proteomic network and cell type changes in Alzheimer's disease. *Front. Mol. Neurosci.* **11**, 454 (2018).
15. L. Higginbotham, E. B. Dammer, D. M. Duong, E. Modeste, T. J. Montine, J. J. Lah, A. I. Levey, N. T. Seyfried, Network analysis of a membrane-enriched brain proteome across stages of Alzheimer's disease. *Proteomes* **7**, 30 (2019).
16. L. Higginbotham, L. Ping, E. B. Dammer, D. M. Duong, M. Zhou, M. Gearing, E. C. B. Johnson, I. Hajjar, J. J. Lah, A. I. Levey, N. T. Seyfried, Integrated proteomics reveals brain-based cerebrospinal fluid biomarkers in asymptomatic and symptomatic Alzheimer's disease. *bioRxiv* , 806752 (2019).
17. E. C. B. Johnson, E. B. Dammer, D. M. Duong, L. Ping, M. Zhou, L. Yin, L. A. Higginbotham, A. Guajardo, B. White, J. C. Troncoso, M. Thambisetty, T. J. Montine, E. B. Lee, J. Q. Trojanowski, T. G. Beach, E. M. Reiman, V. Haroutunian, M. Wang, E. Schadt, B. Zhang, D. W. Dickson, N. Ertekin-Taner, T. E. Golde, V. A. Petyuk, P. L. de Jager, D. A. Bennett, T. S. Wingo, S. Rangaraju, I. Hajjar, J. M. Shulman, J. J. Lah, A. I. Levey, N. T. Seyfried, Large-scale proteomic analysis of Alzheimer's disease brain and cerebrospinal fluid reveals early changes in energy metabolism associated with microglia and astrocyte activation. *Nat. Med.* **26**, 769–780 (2020).
18. E. C. B. Johnson, E. B. Dammer, D. M. Duong, L. Yin, M. Thambisetty, J. C. Troncoso, J. J. Lah, A. I. Levey, N. T. Seyfried, Deep proteomic network analysis of Alzheimer's disease brain reveals alterations in RNA binding proteins and RNA splicing associated with disease. *Mol. Neurodegener.* **13**, 52 (2018).
19. V. Swarup, T. S. Chang, D. M. Duong, E. B. Dammer, J. Dai, J. J. Lah, E. C. B. Johnson, N. T. Seyfried, A. I. Levey, D. H. Geschwind, Identification of conserved proteomic networks in neurodegenerative dementia. *Cell Rep.* **31**, 107807 (2020).
20. A. P. Wingo, E. B. Dammer, M. S. Breen, B. A. Logsdon, D. M. Duong, J. C. Troncosco, M. Thambisetty, T. G. Beach, G. E. Serrano, E. M. Reiman, R. J. Caselli, J. J. Lah, N. T. Seyfried, A. I. Levey, T. S. Wingo, Large-scale proteomic analysis of human brain identifies proteins associated with cognitive trajectory in advanced age. *Nat. Commun.* **10**, 1619 (2019).
21. A. P. Wingo, W. Fan, D. M. Duong, E. S. Gerasimov, E. B. Dammer, Y. Liu, N. V. Harerimana, B. White, M. Thambisetty, J. C. Troncoso, N. Kim, J. A. Schneider, I. M. Hajjar, J. J. Lah, D. A. Bennett, N. T. Seyfried, A. I. Levey, T. S. Wingo, Shared proteomic effects of cerebral atherosclerosis and Alzheimer's disease on the human brain. *Nat. Neurosci.* **23**, 696–700 (2020).
22. Q. Zhang, C. Ma, M. Gearing, P. G. Wang, L.-S. Chin, L. Li, Integrated proteomics and network analysis identifies protein hubs and network alterations in Alzheimer's disease. *Acta Neuropathol. Commun.* **6**, 19 (2018).
23. B. Bai, X. Wang, Y. Li, P.-C. Chen, K. Yu, K. K. Dey, J. M. Yarbro, X. Han, B. M. Lutz, S. Rao, Y. Jiao, J. M. Sifford, J. Han, M. Wang, H. Tan, T. I. Shaw, J.-H. Cho, S. Zhou, H. Wang, M. Niu, A. Mancieri, K. A. Messler, X. Sun, Z. Wu, V. Pagala, A. A. High, W. Bi, H. Zhang, H. Chi, V. Haroutunian, B. Zhang, T. G. Beach, G. Yu, J. Peng, Deep multilayer brain proteomics identifies molecular networks in Alzheimer's disease progression. *Neuron* **105**, 975–991 (2020). e7
24. S. Roche, A. Gabelle, S. Lehmann, Clinical proteomics of the cerebrospinal fluid: Towards the discovery of new biomarkers. *Proteomics Clin. Appl.* **2**, 428–436 (2008).
25. L. Ping, D. M. Duong, L. Yin, M. Gearing, J. J. Lah, A. I. Levey, N. T. Seyfried, Global quantitative analysis of the human brain proteome in Alzheimer's and Parkinson's disease. *Sci. Data* **5**, 180036 (2018).

26. M. E. Umoh, E. B. Dammer, J. Dai, D. M. Duong, J. J. Lah, A. I. Levey, M. Gearing, J. D. Glass, N. T. Seyfried, A proteomic network approach across the ALS-FTD disease spectrum resolves clinical phenotypes and genetic vulnerability in human brain. *EMBO Mol. Med.* **10**, 48–62 (2018).
27. G. Pottiez, L. Yang, T. Stewart, N. Song, P. Aro, D. R. Galasko, J. F. Quinn, E. R. Peskind, M. Shi, J. Zhang, Mass-spectrometry-based method to quantify in parallel tau and amyloid β 1–42 in CSF for the diagnosis of Alzheimer's disease. *J. Proteome Res.* **16**, 1228–1238 (2017).
28. K. G. Mawuenyega, T. Kasten, W. Sigurdson, R. J. Bateman, Amyloid-beta isoform metabolism quantitation by stable isotope-labeled kinetics. *Anal. Biochem.* **440**, 56–62 (2013).
29. Y. Zhang, K. Chen, S. A. Sloan, M. L. Bennett, A. R. Scholze, S. O'Keeffe, H. P. Phatnani, P. Guarnieri, C. Caneda, N. Ruderisch, S. Deng, S. A. Liddelow, C. Zhang, R. Daneman, T. Maniatis, B. A. Barres, J. Q. Wu, An RNA-sequencing transcriptome and splicing database of glia, neurons, and vascular cells of the cerebral cortex. *J. Neurosci.* **34**, 11929–11947 (2014).
30. K. Takeda, S. Akira, Toll-like receptors in innate immunity. *Int. Immunol.* **17**, 1–14 (2005).
31. R. A. Sperling, P. S. Aisen, L. A. Beckett, D. A. Bennett, S. Craft, A. M. Fagan, T. Iwatsubo, C. R. Jack Jr., J. Kaye, T. J. Montine, D. C. Park, E. M. Reiman, C. C. Rowe, E. Siemers, Y. Stern, K. Yaffe, M. C. Carrillo, B. Thies, M. Morrison-Bogorad, M. V. Wagster, C. H. Phelps, Toward defining the preclinical stages of Alzheimer's disease: Recommendations from the National Institute on Aging-Alzheimer's Association workgroups on diagnostic guidelines for Alzheimer's disease. *Alzheimers Dement.* **7**, 280–292 (2011).
32. I. Okada, H. Hamanoue, K. Terada, T. Tohma, A. Megarbane, E. Chouery, J. Abou-Ghoch, N. Jalkh, O. Cogulu, F. Ozkinay, K. Horie, J. Takeda, T. Furuichi, S. Ikegawa, K. Nishiyama, S. Miyatake, A. Nishimura, T. Mizuguchi, N. Niikawa, F. Hirahara, T. Kaname, K. I. Yoshiura, Y. Tsurusaki, H. Doi, N. Miyake, T. Furukawa, N. Matsumoto, H. Saitsu, SMOC1 is essential for ocular and limb development in humans and mice. *Am. J. Hum. Genet.* **88**, 30–41 (2011).
33. J. Kerzerho, O. Adotevi, F. A. Castelli, M. Dosset, K. Bernardeau, N. Szely, F. Lang, E. Tartour, B. Maillere, The angiogenic growth factor and biomarker midkine is a tumor-shared antigen. *J. Immunol.* **185**, 418–423 (2010).
34. M. F. Xiao, D. Xu, M. T. Craig, K. A. Pelkey, C. C. Chien, Y. Shi, J. Zhang, S. Resnick, O. Pletnikova, D. Salmon, J. Brewer, S. Edland, J. Wegiel, B. Tycko, A. Savonenko, R. H. Reeves, J. C. Troncoso, C. J. McBain, D. Galasko, P. F. Worley, NPTX2 and cognitive dysfunction in Alzheimer's disease. *eLife* **6**, e23798 (2017).
35. B. M. Lutz, J. Peng, Deep profiling of the aggregated proteome in Alzheimer's disease: From pathology to disease mechanisms. *Proteomes* **6**, 46 (2018).
36. D. J. Rader, K. A. Dugi, The endothelium and lipoproteins: Insights from recent cell biology and animal studies. *Semin. Thromb. Hemost.* **26**, 521–528 (2000).
37. L. Yi, C. F. Tsai, E. Dirice, A. C. Swensen, J. Chen, T. Shi, M. A. Gritsenko, R. K. Chu, P. D. Piehowski, R. D. Smith, K. D. Rodland, M. A. Atkinson, C. E. Mathews, R. N. Kulkarni, T. Liu, W.-J. Qian, Boosting to amplify signal with isobaric labeling (BASIL) strategy for comprehensive quantitative phosphoproteomic characterization of small populations of cells. *Anal. Chem.* **91**, 5794–5801 (2019).
38. A. S. Hebert, S. Prasad, M. W. Belford, D. J. Bailey, G. C. McAlister, S. E. Abbatiello, R. Huguet, E. R. Wouters, J. J. Dunyach, D. R. Brademan, M. S. Westphall, J. J. Coon, Comprehensive single-shot proteomics with FAIMS on a hybrid orbitrap mass spectrometer. *Anal. Chem.* **90**, 9529–9537 (2018).
39. Y. Sun, X. S. Yin, H. Guo, R. K. Han, R. D. He, L. J. Chi, Elevated osteopontin levels in mild cognitive impairment and Alzheimer's disease. *Mediators Inflamm.* **2013**, 615745 (2013).
40. A. Rentsendorj, J. Sheyn, D. T. Fuchs, D. Daley, B. C. Salumbides, H. E. Schubloom, N. J. Hart, S. Li, E. Y. Hayden, D. B. Teplow, K. L. Black, Y. Koronyo, M. Koronyo-Hamaoui, A novel role for osteopontin in macrophage-mediated amyloid-β clearance in Alzheimer's models. *Brain Behav. Immun.* **67**, 163–180 (2018).
41. C. Comi, M. Carecchio, A. Chiocchetti, S. Nicola, D. Galimberti, C. Fenoglio, G. Cappellano, F. Monaco, E. Scarpini, U. Dianzani, Osteopontin is increased in the cerebrospinal fluid of patients with Alzheimer's disease and its levels correlate with cognitive decline. *J. Alzheimers Dis.* **19**, 1143–1148 (2010).
42. E. Bereczki, R. M. Branca, P. T. Francis, J. B. Pereira, J.-H. Baek, T. Hortobágyi, B. Winblad, C. Ballard, J. Lehtiö, D. Aarsland, Synaptic markers of cognitive decline in neurodegenerative diseases: A proteomic approach. *Brain* **141**, 582–595 (2018).
43. M. I. Kester, C. E. Teunissen, D. L. Crimmins, E. M. Herries, J. H. Ladenson, P. Scheltens, W. M. van der Flier, J. C. Morris, D. M. Holtzman, A. M. Fagan, Neurogranin as a cerebrospinal fluid biomarker for synaptic loss in symptomatic Alzheimer disease. *JAMA Neurol.* **72**, 1275–1280 (2015).
44. A. Thorsell, M. Bjerke, J. Gobom, E. Brunhage, E. Vanmechelen, N. Andreasen, O. Hansson, L. Minthon, H. Zetterberg, K. Blennow, Neurogranin in cerebrospinal fluid as a marker of synaptic degeneration in Alzheimer's disease. *Brain Res.* **1362**, 13–22 (2010).
45. L. Dayon, A. Núñez Galindo, J. Wojcik, O. Cominetti, J. Corthésy, A. Oikonomidi, H. Henry, M. Kussmann, E. Migliavacca, I. Severin, G. L. Bowman, J. Popp, Alzheimer disease pathology and the cerebrospinal fluid proteome. *Alzheimers Res. Ther.* **10**, 66 (2018).
46. L. Dayon, A. Nuñez Galindo, J. Corthésy, O. Cominetti, M. Kussmann, Comprehensive and scalable highly automated MS-based proteomic workflow for clinical biomarker discovery in human plasma. *J. Proteome Res.* **13**, 3837–3845 (2014).
47. I. Driscoll, J. Troncoso, Asymptomatic Alzheimer's disease: A prodrome or a state of resilience? *Curr. Alzheimer Res.* **8**, 330–335 (2011).
48. P. J. Magistretti, I. Allaman, A cellular perspective on brain energy metabolism and functional imaging. *Neuron* **86**, 883–901 (2015).
49. F. Yin, H. Sancheti, I. Patil, E. Cadenas, Energy metabolism and inflammation in brain aging and Alzheimer's disease. *Free Radic. Biol. Med.* **100**, 108–122 (2016).
50. C. V. Ly, P. Verstreken, Mitochondria at the synapse. *Neuroscientist* **12**, 291–299 (2006).
51. S. Hong, V. F. Beja-Glasser, B. M. Nfonoyim, A. Frouin, S. Li, S. Ramakrishnan, K. M. Merry, Q. Shi, A. Rosenthal, B. A. Barres, C. A. Lemere, D. J. Selkoe, B. Stevens, Complement and microglia mediate early synapse loss in Alzheimer mouse models. *Science* **352**, 712–716 (2016).
52. T. Malm, S. Loppi, K. M. Kanninen, Exosomes in Alzheimer's disease. *Neurochem. Int.* **97**, 193–199 (2016).
53. L. Rajendran, M. Honsho, T. R. Zahn, P. Keller, K. D. Geiger, P. Verkade, K. Simons, Alzheimer's disease β-amyloid peptides are released in association with exosomes. *Proc. Natl. Acad. Sci. U.S.A.* **103**, 11172–11177 (2006).
54. S. A. Bellingham, B. B. Guo, B. M. Coleman, A. F. Hill, Exosomes: Vehicles for the transfer of toxic proteins associated with neurodegenerative diseases? *Front. Physiol.* **3**, 124 (2012).
55. M. B. Dinkins, S. Dasgupta, G. Wang, G. Zhu, E. Bieberich, Exosome reduction in vivo is associated with lower amyloid plaque load in the 5XFAD mouse model of Alzheimer's disease. *Neurobiol. Aging* **35**, 1792–1800 (2014).
56. A. Montagne, Z. Zhao, B. V. Zlokovic, Alzheimer's disease: A matter of blood-brain barrier dysfunction? *J. Exp. Med.* **214**, 3151–3169 (2017).
57. A. R. Nelson, M. D. Sweeney, A. P. Sagare, B. V. Zlokovic, Neurovascular dysfunction and neurodegeneration in dementia and Alzheimer's disease. *Biochim. Biophys. Acta* **1862**, 887–900 (2016).
58. C. Aluganti Narasimhulu, C. Mitra, D. Bhardwaj, K. Y. Burge, S. Parthasarathy, Alzheimer's disease markers in aged ApoE-PON1 deficient mice. *J. Alzheimers Dis.* **67**, 1353–1365 (2019).
59. D. A. Chistiakov, A. A. Melnichenko, A. N. Orekhov, Y. V. Bobryshev, Paraoxonase and atherosclerosis-related cardiovascular diseases. *Biochimie* **132**, 19–27 (2017).
60. Y. Shu, R. Li, Y. Yang, Y. Dai, W. Qiu, Y. Chen, Z. Zhao, Z. Lu, X. Hu, Urinary trypsin inhibitor levels are reduced in cerebrospinal fluid of multiple sclerosis and neuromyelitis optica patients during relapse. *Neurochem. Int.* **81**, 28–31 (2015).
61. M. Feng, Y. Shu, Y. Yang, X. Zheng, R. Li, Y. Wang, Y. Dai, W. Qiu, Z. Lu, X. Hu, Ulinastatin attenuates experimental autoimmune encephalomyelitis by enhancing anti-inflammatory responses. *Neurochem. Int.* **64**, 64–72 (2014).
62. M. Zhou, D. M. Duong, E. C. B. Johnson, J. Dai, J. J. Lah, A. I. Levey, N. T. Seyfried, Mass spectrometry-based quantification of tau in human cerebrospinal fluid using a complementary tryptic peptide standard. *J. Proteome Res.* **18**, 2422–2432 (2019).
63. M. Zhou, R. U. Haque, E. B. Dammer, D. M. Duong, L. Ping, E. C. B. Johnson, J. J. Lah, A. I. Levey, N. T. Seyfried, Targeted mass spectrometry to quantify brain-derived cerebrospinal fluid biomarkers in Alzheimer's disease. *Clin. Proteomics* **17**, 19 (2020).
64. J. M. Bader, P. E. Geyer, J. B. Müller, M. T. Strauss, M. Koch, F. Leypoldt, P. Koertvelyessy, D. Bittner, C. G. Schipke, E. I. Incesoy, O. Peters, N. Deigendesch, M. Simons, M. K. Jensen, H. Zetterberg, M. Mann, Proteome profiling in cerebrospinal fluid reveals novel biomarkers of Alzheimer's disease. *Mol. Syst. Biol.* **16**, e9356 (2020).
65. A. Olsson, H. Vanderstichele, N. Andreasen, G. de Meyer, A. Wallin, B. Holmberg, L. Rosengren, E. Vanmechelen, K. Blennow, Simultaneous measurement of β-amyloid$_{(1–42)}$, total tau, and phosphorylated tau (Thr^{181}) in cerebrospinal fluid by the xMAP technology. *Clin. Chem.* **51**, 336–345 (2005).
66. F. Hulstaert, K. Blennow, A. Ivanoiu, H. C. Schoonderwaldt, M. Riemenschneider, P. P. D. Deyn, C. Bancher, P. Cras, J. Wiltfang, P. D. Mehta, K. Iqbal, H. Pottel, E. Vanmechelen, H. Vanderstichele, Improved discrimination of AD patients using β-amyloid$_{(1–42)}$ and tau levels in CSF. *Neurology* **52**, 1555–1562 (1999).
67. L. M. Shaw, H. Vanderstichele, M. Knapik-Czajka, C. M. Clark, P. S. Aisen, R. C. Petersen, K. Blennow, H. Soares, A. Simon, P. Lewczuk, R. Dean, E. Siemers, W. Potter, V. M.-Y. Lee, J. Q. Trojanowski; Alzheimer's disease neuroimaging initiative, Cerebrospinal fluid biomarker signature in Alzheimer's disease neuroimaging initiative subjects. *Ann. Neurol.* **65**, 403–413 (2009).
68. A. Winiarska, L. Zareba, G. Krolczyk, G. Czyzewicz, M. Zabczyk, A. Undas, Decreased levels of histidine-rich glycoprotein in advanced lung cancer: Association with prothrombotic alterations. *Dis. Markers* **2019**, 8170759 (2019).
69. C. L. Russell, A. Heslegrave, V. Mitra, H. Zetterberg, J. M. Pocock, M. A. Ward, I. Pike, Combined tissue and fluid proteomics with tandem mass tags to identify low-abundance protein biomarkers of disease in peripheral body fluid: An Alzheimer's disease case study. *Rapid Commun. Mass Spectrom.* **31**, 153–159 (2017).

70. J. Li, J. G. Van Vranken, L. P. Vaites, D. K. Schweppe, E. L. Huttlin, C. Etienne, P. Nandhikonda, R. Viner, A. M. Robitaille, A. H. Thompson, K. Kuhn, I. Pike, R. D. Bomgarden, J. C. Rogers, S. P. Gygi, J. A. Paulo, TMTpro reagents: A set of isobaric labeling mass tags enables simultaneous proteome-wide measurements across 16 samples. *Nat. Methods* **17**, 399–404 (2020).
71. P. Mertins, L. C. Tang, K. Krug, D. J. Clark, M. A. Gritsenko, L. Chen, K. R. Clauser, T. R. Clauss, P. Shah, M. A. Gillette, V. A. Petyuk, S. N. Thomas, D. R. Mani, F. Mundt, R. J. Moore, Y. Hu, R. Zhao, M. Schnaubelt, H. Keshishian, M. E. Monroe, Z. Zhang, N. D. Udeshi, D. Mani, S. R. Davies, R. R. Townsend, D. W. Chan, R. D. Smith, H. Zhang, T. Liu, S. A. Carr, Reproducible workflow for multiplexed deep-scale proteome and phosphoproteome analysis of tumor tissues by liquid chromatography-mass spectrometry. *Nat. Protoc.* **13**, 1632–1661 (2018).
72. S. S. Mirra, A. Heyman, D. McKeel, S. M. Sumi, B. J. Crain, L. M. Brownlee, F. S. Vogel, J. P. Hughes, G. van Belle, L. Berg; participating CERAD neuropathologists, The Consortium to Establish a Registry for Alzheimer's Disease (CERAD). Part II. Standardization of the neuropathologic assessment of Alzheimer's disease. *Neurology* **41**, 479–486 (1991).
73. H. Braak, E. Braak, Neuropathological stageing of Alzheimer-related changes. *Acta Neuropathol.* **82**, 239–259 (1991).
74. B. T. Hyman, J. Q. Trojanowski, Editorial on consensus recommendations for the postmortem diagnosis of Alzheimer disease from the national institute on aging and the reagan institute working group on diagnostic criteria for the neuropathological assessment of Alzheimer disease. *J. Neuropathol. Exp. Neurol.* **56**, 1095–1097 (1997).
75. D. F. Brown, M. A. Dababo, E. H. Bigio, R. C. Risser, K. P. Eagan, C. L. Hladik, C. L. White III, Neuropathologic evidence that the Lewy body variant of Alzheimer disease represents coexistence of Alzheimer disease and idiopathic Parkinson disease. *J. Neuropathol. Exp. Neurol.* **57**, 39–46 (1998).
76. M. Narayanan, J. L. Huynh, K. Wang, X. Yang, S. Yoo, J. McElwee, B. Zhang, C. Zhang, J. R. Lamb, T. Xie, C. Suver, C. Molony, S. Melquist, A. D. Johnson, G. Fan, D. J. Stone, E. E. Schadt, P. Casaccia, V. Emilsson, J. Zhu, Common dysregulation network in the human prefrontal cortex underlies two neurodegenerative diseases. *Mol. Syst. Biol.* **10**, 743 (2014).
77. A. C. Zambon, S. Gaj, I. Ho, K. Hanspers, K. Vranizan, C. T. Evelo, B. R. Conklin, A. R. Pico, N. Salomonis, GO-Elite: A flexible solution for pathway and ontology over-representation. *Bioinformatics* **28**, 2209–2210 (2012).

Acknowledgments

Funding: Support for this research was provided by funding from the National Institute on Aging (R01AG053960, R01AG057911, R01AG061800, RF1AG057471, RF1AG057470, R01AG061800, R01AG057911, and R01AG057339), the Accelerating Medicine Partnership for AD (U01AG046161 and U01AG061357), the Emory ADRC (P50AG025688), and the NINDS Emory Neuroscience Core (P30NS055077). Support was also provided by the Foundation for the National Institutes of Health (FNIH). N.T.S. was also supported in part by grants from the Alzheimer's Association (ALZ), Alzheimer's Research UK (ARUK), The Michael J. Fox Foundation for Parkinson's Research (MJFF), and the Weston Brain Institute (11060). **Author contributions:** Conceptualization: L.H., E.B.D., E.C.B.J., J.J.L., A.I.L., and N.T.S. Methodology: L.H., L.P., E.B.D., D.M.D., and N.T.S. Investigation: L.H., L.P., E.B.D., D.M.D., M.Z., C.H., and N.T.S. Formal analysis: E.B.D. Writing (original draft): L.H., L.P., and E.B.D. Writing (review and editing): L.H., E.C.B.J., J.J.L., A.I.L., and N.T.S. Funding acquisition: A.I.L. and N.T.S. Resources: M.G., I.H., J.D.G., S.A.F., and J.J.L. Supervision: A.I.L., J.J.L., and N.T.S. **Competing interests:** N.T.S., A.I.L., J.J.L., L.H., and D.M.D are co-inventors on the U.S. patent application no. 62/912,841 titled "CSF biomarker panels that reflect Alzheimer's disease brain pathology and response to drug treatment" was filed 9 October 2019 by Emory University as a provisional patent. The authors declare that they have no other competing interests. **Data and materials availability:** All data needed to evaluate the conclusions in the paper are present in the paper and/or the Supplementary Materials. All raw proteomic data contributing to the described work will be deposited electronically on SYNAPSE (https://synapse.org/#!Synapse:syn20821165/wiki/596086) in accordance with the data sharing policies of the AMP-AD. Specific software will also be made available upon request. Additional data related to this paper may be requested from the authors.

Submitted 21 October 2019
Accepted 3 September 2020
Published 21 October 2020
10.1126/sciadv.aaz9360

Citation: L. Higginbotham, L. Ping, E. B. Dammer, D. M. Duong, M. Zhou, M. Gearing, C. Hurst, J. D. Glass, S. A. Factor, E. C. B. Johnson, I. Hajjar, J. J. Lah, A. I. Levey, N. T. Seyfried, Integrated proteomics reveals brain-based cerebrospinal fluid biomarkers in asymptomatic and symptomatic Alzheimer's disease. *Sci. Adv.* **6**, eaaz9360 (2020).